

Article

An ADCP Attitude Dynamic Errors Correction Method Based on Angular Velocity Tensor and Radius Vector Estimation

Zhaowen Sun ¹, Shuai Yao ^{1,*} , Ning Gao ² and Ke Zhang ³¹ Key Laboratory of Underwater Acoustic Signal Processing, Ministry of Education, Southeast University, Nanjing 210096, China; szw161618@163.com² School of Cyber Science and Engineering, Southeast University, Nanjing 210096, China; ninggao@seu.edu.cn³ Guobo Electronics Co., Ltd., Nanjing 211111, China

* Correspondence: 101012104@seu.edu.cn

Abstract: An acoustic Doppler current profiler (ADCP) installed on a platform produces rotational tangential velocity as a result of variations in the platform's attitude, with both the tangential velocity and radial orientation varying between each pulse's transmission and reception by the transducer. These factors introduce errors into the measurements of vessel velocity and flow velocity. In this study, we address the errors induced by dynamic factors related to variations in attitude and propose an ADCP attitude dynamic error correction method based on angular velocity tensor and radius vector estimation. This method utilizes a low-sampling-rate inclinometer and compass data and estimates the angular velocity tensor based on a physical model of vessel motion combined with nonlinear least-squares estimation. The angular velocity tensor is then used to estimate the transducers' radius vectors. Finally, the radius vectors are employed to correct the instantaneous tangential velocity within the measured velocities of the vessel and flow. To verify the effectiveness of the proposed method, field tests were conducted in a water pool. The results demonstrate that the proposed method surpasses the attitude static correction approach. In comparison with the ASC method, the average relative error in vessel velocity during free-swaying movement decreased by 20.94%, while the relative standard deviation of the error was reduced by 17.38%.

Keywords: ADCP; swaying platform; attitude dynamic error correction; angular velocity tensor estimation; radius vector estimation; instantaneous tangential velocity correction



Citation: Sun, Z.; Yao, S.; Gao, N.; Zhang, K. An ADCP Attitude Dynamic Errors Correction Method Based on Angular Velocity Tensor and Radius Vector Estimation. *J. Mar. Sci. Eng.* **2024**, *12*, 2018. <https://doi.org/10.3390/jmse12112018>

Academic Editor: Sergei Chernyi

Received: 25 September 2024

Revised: 30 October 2024

Accepted: 5 November 2024

Published: 8 November 2024



Copyright: © 2024 by the authors. Licensee MDPI, Basel, Switzerland. This article is an open access article distributed under the terms and conditions of the Creative Commons Attribution (CC BY) license (<https://creativecommons.org/licenses/by/4.0/>).

1. Introduction

The acoustic Doppler current profiler (ADCP) is an instrument that measures flow velocity profiles by utilizing the Doppler effect of sound waves. In the development of deep-sea oil and gas resources [1], biological and environmental observations [2], ocean-current scientific research [3], underwater warfare [4], long-term wave observation in coastal areas [5], fishery management [6], freshwater fishery research in rivers and lakes [7], and river hydrological studies [8], water flow velocity information is indispensable. Among various flow measurement devices, the ADCP is the most commonly used instrument for flow velocity measurement [9] because it can simultaneously measure water flow velocity at all detected depths, offering advantages such as convenience, speed, and non-interference with the measured fluid [10].

Based on differences in their installation platforms, installation methods, application scenarios, and data-reading methods, ADCPs are divided into several distinct types [11]. The commonly used vessel-installed ADCPs, which include shipborne and towed types, can be mounted on platforms like ships, buoys [12], and AUVs [13] and serve to measure both vessel velocity and flow velocity profiles [14]. Compared with conventional flow measurement instruments, vessel-installed ADCPs offer the advantages of fast measurement speed and flexible, convenient operation while also eliminating the high costs and responsibilities

associated with constructing and maintaining expensive cableways. These advantages have led to its widespread application in fields such as ocean exploration, hydrological measurement, and experimental research, providing significant convenience [15].

When the platform's attitude shifts, the ADCP mounted on it undergoes corresponding attitude changes, leading to variations in the radial velocity components of each transducer, which impacts the accuracy of vessel and flow velocity measurements. To address this, vessel-installed ADCPs are generally equipped with inclinometers and electronic compasses to correct for tilt angles and to ascertain the navigation direction, thereby transforming vessel velocity, flow velocity, and depth coordinates from the transducer system into the Earth coordinate system [16,17].

In reality, the changes in attitude not only result in differences in angles at two moments but also generate angular velocity during the angle change, which, in turn, produces rotational tangential velocity in addition to the vessel's navigation velocity. Typically, the influence of ADCP attitude changes is corrected for by compensating for the attitude's tilt angle, which often overlooks the impact of tangential velocity generated by the transducer's motion. Some researchers suggest that the effect of tangential velocity can be entirely ignored when the vessel's roll amplitude is within 5° [18], while others posit that the symmetrical Janus [19] transducer structure compensates for the swaying effects. In such instances, the dynamic effects of swaying may occasionally be negligible, allowing conventional ADCP attitude correction methods to produce acceptable results. Nevertheless, in specific cases, the impact of the transducer's swaying tangential velocity on vessel and flow velocity measurements can be considerable.

For example, in towed ADCPs mounted on small boats, the swaying period is generally short, and the angular velocity is fast. For small boats with a scale of about 3 m, the swaying period is approximately 1 s, which results in considerable transducer tangential velocity, potentially causing vessel and flow velocity measurement errors that exceed 0.1 m/s and 0.01 m/s, respectively. For larger vessels, although the swaying period is longer and the angular velocity is smaller, the large swaying radius may still generate significant tangential velocity for the transducers. Similarly, in deep-sea ocean observations, typically conducted via moored systems, current measurement instruments within the buoy system experience tilting and swaying due to the water flow. This motion affects flow measurement accuracy due to the displacement, attitude shifts, and the tangential velocity induced by these changes [12,20]. Furthermore, given the time interval between the ADCP pulse transmission (TX) and reception (RX), if the pulse round-trip time aligns closely with the swaying period, variations in the tangential velocity and the transducers' radial direction during this interval may also influence the velocity measurements.

Thus, conventional ADCPs address only the static components of attitude changes, overlooking variations in attitude and velocity during echo TX and RX. To distinguish it from conventional correction approaches, we term the method that corrects solely for static attitude factors as the "attitude static correction method", while the approach that also accounts for additional tangential velocity due to swaying and other dynamic attitude factors is referred to as the "attitude dynamic correction method". For simplicity and convenience, we abbreviate the "attitude static correction method" as the "ASC method" and the "attitude dynamic correction method" as the "ADC method".

A number of scholars have explored approaches to mitigate the effects of platform swaying dynamics on the accuracy of flow measurements. For instance, in [21], when using an ADCP to measure sediment transport velocity, the influence of the swaying-induced tangential velocity was noted, but due to a limited understanding of acoustic principles, the transducer TX and RX, and pulse characteristics, no correction for swaying effects was applied. In [22], inertial navigation and differential GPS data were applied to correct ADCP-measured water flow velocities, effectively reducing the impact of vessel swaying and yielding high-quality single-ping ADCP data with enhanced spatiotemporal resolution. However, this approach did not consider variations in tangential velocity and radial orientation within a single pulse TX and RX cycle. In [23], while researching acoustic

array installation error correction, a formula was derived for calculating vessel speed when the array installation deviates from the swaying center, introducing additional tangential velocity due to swaying. However, this approach treated the array as a point mass, ignoring the differing velocities of individual transducers and changes in velocity at the TX and RX times. In [24], a differential GPS was used to correct the ADCP velocity measurements by considering tangential velocity effects, but changes in tangential velocity during each ping due to swaying were not accounted for. Additionally, a differential GPS has high operational costs, requires a reference station setup in open areas with good GPS signals, is limited by distance (typically up to 10 km for RTK), and has a low data-update rate (generally 1–20 Hz).

Some of the aforementioned studies have yielded significant results in tangential velocity correction; however, they necessitate the use of additional devices, such as an inertial navigation system (INS), differential GPS, or attitude and heading reference system (AHRS), during measurements. This requirement increases both the cost and complexity of flow measurements, thus limiting their flexibility and ease of use. Furthermore, these methods do not account for the variations in tangential velocity and radial orientation during each pulse TX and RX.

To address the shortcomings of the above methods, we propose an ADCP attitude dynamic error correction method based on angular velocity tensor and radius vector estimation. This method considers the effects of attitude dynamics as well as the variations in tangential velocity and radial orientation between pulse TX and RX. First, the angular velocity tensor is estimated using a physical model of vessel motion combined with the nonlinear least-squares method. Then, the radius vectors of the transducers are estimated using the angular velocity tensor. Finally, the radius vectors are utilized to correct for the instantaneous tangential velocity within the measured vessel and flow velocities. This method is intended for typical application scenarios in which the ADCP is mounted on a freely swaying vessel and the measurements are performed in calm wave-free water; for instance, when towing the vessel across a relatively calm lake or reservoir.

In comparison with other related studies, this method solely processes data measured by the ADCP, eliminating the need for additional attitude measurement or navigation equipment. It also accounts for changes in tangential velocity and radial orientation during each pulse TX and RX, thereby providing instantaneous tangential velocity correction for both the vessel and the flow velocities. While more sophisticated attitude dynamic error correction techniques requiring additional equipment are widely used in ship and vehicle navigation systems, they are less common in the ADCP field. Furthermore, the majority of these sophisticated methods depend on supplementary attitude measurement or navigation equipment. Additionally, although large sea vessels often have precise, high-speed motion sensors, ADCPs are frequently used in rivers, lakes, and other water bodies where smaller vessels typically lack such sensors. The method proposed in this study is also suitable for post-processing previously collected ADCP data that lack attitude dynamic error correction or precise high-speed attitude information, providing a means to retroactively correct dynamic errors and to recover the value of existing data.

The remainder of this paper is organized as follows: Section 2 mainly derives the motion parameters of the vessel and transducers and introduces the physical model of vessel motion along with the empirical formulas for its parameters, laying the foundation for the derivation of the proposed method. Section 3 presents the principles and derivation process of the proposed method. Section 4 validates the effectiveness of the proposed method through water pool experiments and compares its performance with the ASC method. Section 5 discusses the limitations of the proposed method and its potential for expanded applications. Section 6 concludes the paper with a summary.

2. Preliminaries

This section primarily establishes the transducer, vessel, and Earth coordinate systems; derives the motion parameters of the vessel and transducers; and introduces the physical

model of vessel motion and empirical formulas for its parameters, laying the groundwork for the derivation of the proposed method.

This paper focuses exclusively on the case of four transducers arranged in a Janus configuration. For phased-array transducers, the term “transducer” later in this paper refers to discrete transducers that, after beamforming, are equivalent to the phased-array transducer. Notably, the central axis of the four transducers denotes the symmetrical axis of their acoustic axes, where each acoustic axis is the centerline of the respective transducer’s acoustic beam.

2.1. Establishment of Coordinate Systems and Coordinate System Transformation

This section establishes the transducer, vessel, and Earth coordinate systems and provides the transformation matrices between these coordinate systems to prepare for the subsequent derivations. The conventional ADCP attitude correction method (ASC method) is also briefly introduced to establish a basis for comparing the performance of the methods.

As shown in Figure 1, the Earth coordinate system $Oxyz$, the vessel coordinate system $Gx_b y_b z_b$, and the transducer coordinate system $Px_t y_t z_t$ are established, where G is the center of mass of the vessel. P represents the center of the four transducers, which are arranged as depicted in the lower right corner of Figure 1. The x_t axis and y_t axis pass through the centers of transducers 1 and 2 and transducers 4 and 3, respectively, while the z_t axis points outward. The distance between the center of each transducer (1, 2, 3, and 4) and the origin P is tr . The angle between the acoustic axis of each transducer and the z_t axis is α , and the projection of the acoustic axis of each transducer onto the $x_t y_t$ plane forms an angle β with the positive direction of the x_t axis.

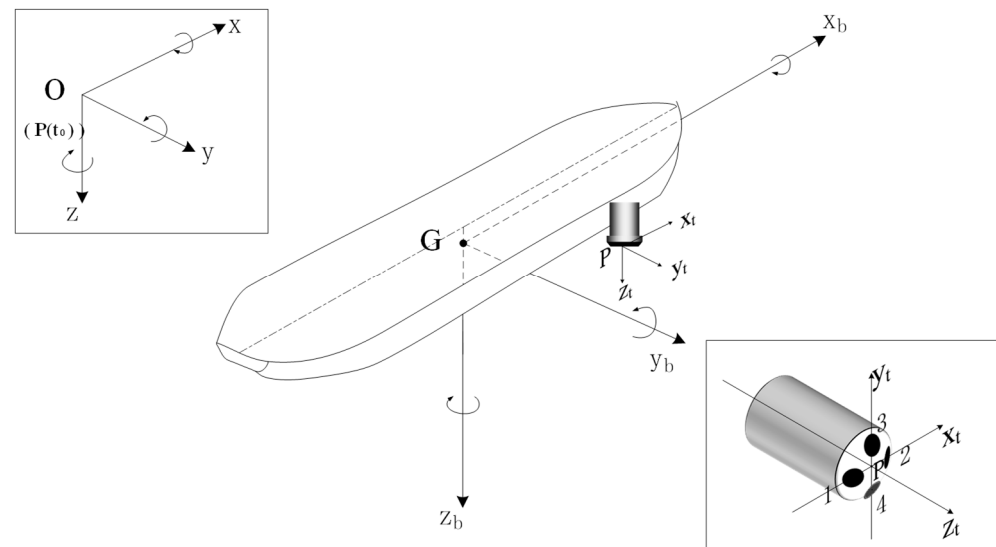


Figure 1. The Earth coordinate system $Oxyz$, the vessel (body-fixed) coordinate system $Gx_b y_b z_b$, and the transducer coordinate system $Px_t y_t z_t$.

The depth of the origin O of the Earth coordinate system $Oxyz$ (distance from the water surface) is H_O , while the water depth is H , and the observed depth is H_n . The yaw, pitch, and roll angles of the transducer coordinate system $Px_t y_t z_t$ relative to the vessel coordinate system $Gx_b y_b z_b$ are ψ_{tb} , θ_{tb} , and ϕ_{tb} , respectively. The direction vector along the outward transducer acoustic axis in the transducer coordinate system $Px_t y_t z_t$ is \vec{d}_{Tt} . The transmission time is t_T , and the yaw, pitch, and roll angles of the vessel coordinate system $Gx_b y_b z_b$ relative to the Earth coordinate system $Oxyz$, as measured by the inclinometer and electronic compass, are ψ , θ , and ϕ , respectively. The radial direction is defined as the outward direction along the acoustic axis. In the ASC method, since variations in the radial

direction throughout the TX and RX time intervals are not considered, the radial direction at the transmission time t_T is typically taken as the radial direction for the entire ping.

For convenience, we abbreviate “the bottom-tracking radial velocities” as “the BT radial velocities”. Let the BT radial velocities of the four beams measured by the conventional ADCP and the radial components of the flow velocity at depth H_n relative to the transducers be denoted, respectively, as

$$\vec{V}_{BTRadTraAll} = [V_{BTRad1}, V_{BTRad2}, V_{BTRad3}, V_{BTRad4}]^T, \quad (1)$$

$$\vec{V}_{n1RadTraAll} = [V_{n1Rad1}, V_{n1Rad2}, V_{n1Rad3}, V_{n1Rad4}]^T, \quad (2)$$

where $V_{BTRad1}, V_{BTRad2}, V_{BTRad3}, V_{BTRad4}$ represent the radial BT velocity scalars of the four transducers, and $V_{n1Rad1}, V_{n1Rad2}, V_{n1Rad3}, V_{n1Rad4}$ denote the radial relative flow velocity scalars of the four transducers. The radial component of the flow velocity at depth H_n is expressed as

$$\vec{V}_{nRadTraAll} = [V_{nRad1}, V_{nRad2}, V_{nRad3}, V_{nRad4}]^T. \quad (3)$$

Thus, by subtracting the bottom-tracking radial velocity $\vec{V}_{BTRadTraAll}$ from the radial flow velocity relative to the transducers $\vec{V}_{n1RadTraAll}$, the radial flow velocity relative to the Earth $\vec{V}_{nRadTraAll}$ is obtained as follows:

$$\vec{V}_{nRadTraAll} = \vec{V}_{n1RadTraAll} - \vec{V}_{BTRadTraAll}. \quad (4)$$

The formula for converting the four-beam radial velocities into the transducer coordinate system is given as follows [25]:

$$\Lambda_{beamt} = \begin{bmatrix} -\frac{\cos \beta}{2 \sin \alpha} & \frac{\cos \beta}{2 \sin \alpha} & -\frac{\sin \beta}{2 \sin \alpha} & \frac{\sin \beta}{2 \sin \alpha} \\ -\frac{\sin \beta}{2 \sin \alpha} & \frac{\sin \beta}{2 \sin \alpha} & \frac{\cos \beta}{2 \sin \alpha} & -\frac{\cos \beta}{2 \sin \alpha} \\ \frac{1}{4 \cos \alpha} & \frac{1}{4 \cos \alpha} & \frac{1}{4 \cos \alpha} & \frac{1}{4 \cos \alpha} \end{bmatrix}. \quad (5)$$

The transformation matrix from the transducer coordinate system $Px_t y_t z_t$ to the vessel coordinate system $Gx_b y_b z_b$, denoted as Λ_{tb} , and the transformation matrix from the vessel coordinate system $Gx_b y_b z_b$ to the Earth coordinate system $Oxyz$, denoted as $\Lambda(t)$, are given as follows [26]:

$$\Lambda_{tb} = \begin{bmatrix} \cos \psi_{tb} \cos \theta_{tb} & \cos \psi_{tb} \sin \theta_{tb} \sin \phi_{tb} - \sin \psi_{tb} \cos \phi_{tb} & \cos \psi_{tb} \sin \theta_{tb} \cos \phi_{tb} + \sin \psi_{tb} \sin \phi_{tb} \\ \sin \psi_{tb} \cos \theta_{tb} & \sin \psi_{tb} \sin \theta_{tb} \sin \phi_{tb} + \cos \psi_{tb} \cos \phi_{tb} & \sin \psi_{tb} \sin \theta_{tb} \cos \phi_{tb} - \cos \psi_{tb} \sin \phi_{tb} \\ -\sin \theta_{tb} & \cos \theta_{tb} \sin \phi_{tb} & \cos \theta_{tb} \cos \phi_{tb} \end{bmatrix}, \quad (6)$$

$$\Lambda(t) = \begin{bmatrix} \cos \psi \cos \theta & \cos \psi \sin \theta \sin \phi - \sin \psi \cos \phi & \cos \psi \sin \theta \cos \phi + \sin \psi \sin \phi \\ \sin \psi \cos \theta & \sin \psi \sin \theta \sin \phi + \cos \psi \cos \phi & \sin \psi \sin \theta \cos \phi - \cos \psi \sin \phi \\ -\sin \theta & \cos \theta \sin \phi & \cos \theta \cos \phi \end{bmatrix}. \quad (7)$$

Thus, the BT velocity \vec{V}_{BTRa} and flow velocity at depth H_n , \vec{V}_{nTra} , within the Earth coordinate system $Oxyz$, obtained using the ASC method, are given as follows:

$$\vec{V}_{BTRa} = \Lambda(t) \Lambda_{tb} \Lambda_{beamt} \vec{V}_{BTRadTraAll}, \quad (8)$$

$$\vec{V}_{nTra} = \Lambda(t) \Lambda_{tb} \Lambda_{beamt} \vec{V}_{nRadTraAll}. \quad (9)$$

The correction process of the aforementioned ASC method clearly reveals that it fails to consider the tangential velocity generated by platform swaying as well as variations in the tangential velocity and radial orientation during echo TX and RX, both of which introduce errors. Next, based on the established three coordinate systems and the transformation

matrices, the motion parameters of the vessel and transducers required for the proposed method will be derived.

2.2. Vessel and Transducer Motion Parameters

Let the yaw angle, pitch angle, and roll angle of the vessel coordinate system $Gx_b y_b z_b$ relative to the Earth coordinate system at time t be $\psi(t)$, $\theta(t)$, and $\phi(t)$, respectively. At time t_0 , when point P passes through point O , the roll angle is $\phi(t_0)$.

Assume that the navigation velocity \vec{V}_a (velocity in the equilibrium coordinate system) remains constant during a single pulse TX and RX. At the initial time t_0 , the vessel's bow is pointing in the x direction, meaning that the x_b axis is aligned with the x axis.

Taking transducer 2 as an example, let t_0 be the time when the pulse transmission begins and the position vector of the center of the four transducers be $\vec{P}(t)$. At time t_0 , $\vec{P}(t_0)$ is at the origin O . The position vector of transducer 2 is denoted as $\vec{T}_2(t)$. Let the velocity of the center of the four transducers P be $\vec{V}(t)$ and the velocity of transducer 2 be $\vec{V}_{T_2}(t)$. The position vectors $\vec{P}(t)$ and $\vec{T}_2(t)$, as functions of time t , are the sum vectors of their respective navigation displacement and swaying displacement.

The angular oscillations of the vessel along the longitudinal, lateral, and vertical axes through the center of gravity G are referred to as the roll, pitch, and yaw, respectively. The roll angle ϕ is defined as the angle between the plane $x_b G z_b$ and the vertical plane passing through the $G x_b$ axis, with the positive direction being counterclockwise as viewed from the bow to the stern. The position vector of point P in the vessel coordinate system is $\vec{P}_b(P_{xb}, P_{yb}, P_{zb})^T$. The angle ϕ_{bP} between the projection of GP_b on the $y_b G z_b$ plane and the z_b axis is $\arctan(-P_{yb}/P_{zb})$. Since at time t_0 , the x_b axis is aligned with the x axis and point P is at the origin O , and because the center of gravity G does not sway with the vessel, the position vector of the center of gravity $\vec{G}(t)$ is given by

$$\vec{G}(t) = \vec{G}(t_0) + \vec{V}_a(t - t_0), \quad (10)$$

where

$$\vec{G}(t_0) = (-P_{xb}, R \sin[\phi_{bP} + \phi(t_0)], -R \cos[\phi_{bP} + \phi(t_0)])^T. \quad (11)$$

Taking the time derivative of $\vec{G}(t)$ gives the navigation velocity \vec{V}_a , which is expressed as

$$\vec{V}_a = \dot{\vec{G}}(t). \quad (12)$$

Next, the transformation matrices between the three-coordinate systems will be used to calculate the motion position vectors.

The position vector of transducer 2 in the transducer coordinate system is given by

$$\vec{T}_{2t} = (tr, 0, 0)^T. \quad (13)$$

Thus, its position vector in the vessel coordinate system, denoted as \vec{T}_{2b} , is given by

$$\vec{T}_{2b} = \Lambda_{tb} \vec{T}_{2t} + \vec{P}_b. \quad (14)$$

The position vector of transducer 2 in the Earth coordinate system, denoted as $\vec{T}_2(t)$, is given by

$$\vec{T}_2(t) = \Lambda(t) \vec{T}_{2b} + \vec{G}(t). \quad (15)$$

The position vectors of transducers 1, 3, and 4 in the $Px_t y_t z_t$ coordinate system are given as follows:

$$\vec{T}_{1t} = (-tr, 0, 0)^T, \quad (16)$$

$$\vec{T}_{3t} = (0, tr, 0)^T, \quad (17)$$

$$\vec{T}_{4t} = (0, -tr, 0)^T. \quad (18)$$

Similarly, the position vectors of transducers 1, 3, and 4 in the Earth coordinate system are given by

$$\vec{T}_i(t) = \Lambda(t) \vec{T}_{ib} + \vec{G}(t). \quad (19)$$

Here, i takes the values 1, 3, and 4, and i also takes the values 1, 3, and 4 in the following Equations (20)–(24). In the above equation,

$$\vec{T}_{ib} = \Lambda_{tb} \vec{T}_{it} + \vec{P}_b. \quad (20)$$

Similarly, the position vector $\vec{P}(t)$ can be expressed as

$$\vec{P}(t) = \Lambda(t) \vec{P}_b + \vec{G}(t). \quad (21)$$

According to Equation (12), differentiating $\vec{T}_2(t)$ and $\vec{P}(t)$ yields the velocities of transducer 2 and point P , denoted as $\vec{V}_{T_2}(t)$ and $\vec{V}(t)$, respectively, which are given by:

$$\begin{aligned} \vec{V}_{T_2}(t) &= \dot{\vec{T}}_2(t) \\ &= \dot{\Lambda}(t) \vec{T}_{2b} + \dot{\vec{G}}(t) \\ &= \dot{\Lambda}(t) \left(\Lambda_{tb} \vec{T}_{2t} + \vec{P}_b \right) + \vec{V}_a(t), \end{aligned} \quad (22)$$

$$\begin{aligned} \vec{V}(t) &= \dot{\vec{P}}(t) \\ &= \dot{\Lambda}(t) \vec{P}_b + \vec{V}_a(t). \end{aligned} \quad (23)$$

Similarly, the velocities of transducers 1, 3, and 4 are given by

$$\vec{V}_{Ti}(t) = \dot{\Lambda}(t) \left(\Lambda_{tb} \vec{T}_{it} + \vec{P}_b \right) + \vec{V}_a(t). \quad (24)$$

Since the radial direction of all four transducers forms an angle of α with the z_t axis, the transmission direction vector of transducer 2 in the transducer coordinate system, $\vec{d}_{T2t}(t)$, is given by

$$\vec{d}_{T2t}(t) = (\sin \alpha, 0, \cos \alpha)^T. \quad (25)$$

Thus, the transmission direction (radial) unit vector of transducer 2 in the Earth coordinate system, denoted as $\vec{d}_{T2}(t)$, is given by

$$\begin{aligned} \vec{d}_{T2}(t) &= \Lambda(t) \left[\Lambda_{tb} (\sin \alpha, 0, \cos \alpha)^T + \vec{p}_b \right] + \\ &\quad \vec{G}(t) - \left\{ \Lambda(t) \left[\Lambda_{tb} (0, 0, 0)^T + \vec{p}_b \right] + \vec{G}(t) \right\} \\ &= \Lambda(t) \Lambda_{tb} (\sin \alpha, 0, \cos \alpha)^T. \end{aligned} \quad (26)$$

Similarly, the transmission direction (radial) unit vectors of transducers 1, 3, and 4 as functions of time are given by:

$$\vec{d}_{T1}(t) = \Lambda(t)\Lambda_{tb}(-\sin\alpha, 0, \cos\alpha)^T, \quad (27)$$

$$\vec{d}_{T3}(t) = \Lambda(t)\Lambda_{tb}(0, \sin\alpha, \cos\alpha)^T, \quad (28)$$

$$\vec{d}_{T4}(t) = \Lambda(t)\Lambda_{tb}(0, -\sin\alpha, \cos\alpha)^T. \quad (29)$$

At this point, the time-dependent relationships for the position vectors $\vec{T}_1(t)$, $\vec{T}_2(t)$, $\vec{T}_3(t)$, and $\vec{T}_4(t)$; the time-dependent velocity relationships $\vec{V}_{T1}(t)$, $\vec{V}_{T2}(t)$, $\vec{V}_{T3}(t)$, and $\vec{V}_{T4}(t)$; and the time-dependent transmission direction (radial) unit vectors $\vec{d}_{T1}(t)$, $\vec{d}_{T2}(t)$, $\vec{d}_{T3}(t)$, and $\vec{d}_{T4}(t)$ of transducers 1, 2, 3 and 4, installed at arbitrary positions and orientations on the vessel, have been determined.

Let the tangential velocity vector of transducer 2 be \vec{V}_{T2Sw} and the radius vector be \vec{r}_{T2} . Since G is both the origin of the vessel coordinate system and the vessel's center of gravity, which is also the center of rotation during swaying, we have

$$\vec{r}_{T2} = \vec{T}_{2b}. \quad (30)$$

Since the angular velocity tensor can be directly used to calculate the tangential velocity of any point on a rigid body and is particularly suited for describing complex rotational motion, we now introduce the angular velocity tensor. Let the angular velocity tensor corresponding to the vessel's swaying motion be denoted as Ω . According to the relationship between the angular velocity tensor and the tangential velocity, we have

$$\vec{V}_{T2Sw} = \Omega \vec{r}_{T2}. \quad (31)$$

According to the rotational motion of a rigid body and the transformation rules between different coordinate systems, Ω can be obtained from the transformation matrix $\Lambda(t)$ of the vessel coordinate system to the Earth coordinate system. The formula is as follows:

$$\Omega = \dot{\Lambda}(t)\Lambda^T(t). \quad (32)$$

The corresponding angular velocity vector is given by

$$\vec{\omega} = [\dot{\phi}(t), \dot{\theta}(t), \dot{\psi}(t)]^T. \quad (33)$$

Next, we introduce the physical model of vessel motion that is required for estimating the angular velocity tensor, along with the empirical formulas for the parameters involved.

2.3. Physical Model of Vessel Motion

A. Roll Motion Model

As shown in Figure 2, the body-fixed coordinate system and the schematic diagram of the ship's roll, pitch, and yaw are illustrated. Point G represents the ship's center of gravity.

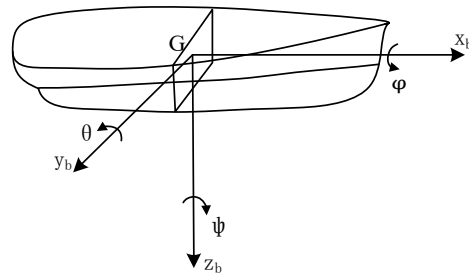


Figure 2. Schematic diagram of vessel swaying.

Assuming the vessel undergoes a small-angle roll motion in still water, at the initial time $t = t_{0r}$, we have $\varphi = \varphi_0$ and $\dot{\varphi} = 0$. The damped roll motion equation is given by [27]

$$\varphi = \varphi_0 e^{-v_{\varphi\varphi}(t-t_{0r})} \left[\cos n_{\varphi_1}(t-t_{0r}) + \frac{v_{\varphi\varphi}}{n_{\varphi_1}} \sin n_{\varphi_1}(t-t_{0r}) \right], \quad (34)$$

where

$$n_{\varphi_1} = \sqrt{n_{\varphi}^2 - v_{\varphi\varphi}^2} \quad (35)$$

is the damped roll natural circular frequency of the vessel, $J_{\varphi\varphi}$ is the moment of inertia about the central principal axis Gx_b , $\Delta J_{\varphi\varphi}$ is the added moment of inertia about the central principal axis Gx_b , $2N_{\varphi\varphi}$ is the roll damping coefficient (damping moment coefficient), and n_{φ} is the approximate natural circular frequency of free roll motion (without damping), given by

$$n_{\varphi} = \sqrt{\frac{Dh}{J_{\varphi\varphi} + \Delta J_{\varphi\varphi}}}, \quad (36)$$

where D is the vessel's displacement, h is the metacentric height, and $2v_{\varphi\varphi}$ is the roll decay coefficient, given by

$$2v_{\varphi\varphi} = \frac{2N_{\varphi\varphi}}{J_{\varphi\varphi} + \Delta J_{\varphi\varphi}}. \quad (37)$$

For common vessel types, the empirical formula for the roll moment of inertia $J_{\varphi\varphi}$ can be expressed as

$$J_{\varphi\varphi} = k_1 \cdot m \cdot B^2, \quad (38)$$

where k_1 is an empirical coefficient, typically between 0.2 and 0.3, m is the total mass of the vessel, and B is the width of the vessel.

The empirical formula for the added roll moment of inertia $\Delta J_{\varphi\varphi}$ is given by

$$\Delta J_{\varphi\varphi} = k_2 \cdot \rho \cdot V \cdot L^2, \quad (39)$$

where k_2 is an empirical coefficient, with values of 0.1, 0.2, and 0.15 for short and broad, slender, and flat-bottomed hulls, respectively; ρ is the density of water; V is the displacement volume of the hull; and L is the length of the hull.

For fishing vessels and small ships, the empirical formula for the roll damping coefficient $2N_{\varphi\varphi}$ is given by

$$2N_{\varphi\varphi} = k_3 \cdot \rho \cdot B \cdot T_s^2 \cdot \sqrt{B}, \quad (40)$$

where k_3 is an empirical coefficient, typically ranging between 0.03 and 0.08, and T_s is the draft (depth of the vessel below the waterline).

B. Pitch Motion Model

Assuming the pitch motion is small, at time $t = t_{0p}$, we have $\theta = \theta_0$ and $\dot{\theta} = 0$. The pitch motion equation is given by [27]

$$\theta = \theta_a e^{-v_{\theta\theta}(t-t_{0p})} \cos[n_{\theta_1}(t-t_{0p}) - \varepsilon_\theta], \quad (41)$$

where n_{θ_1} is the damped natural circular frequency of the vessel's pitch motion, and

$$\begin{aligned} n_{\theta_1} &= \sqrt{n_\theta^2 - v_{\theta\theta}^2}, \\ \theta_a &= \theta_0 \sqrt{1 + \left(\frac{v_{\theta\theta}}{n_{\theta_1}}\right)^2}, \\ \varepsilon_\theta &= \tan^{-1}\left(\frac{v_{\theta\theta}}{n_{\theta_1}}\right). \end{aligned} \quad (42)$$

The pitch damping coefficient $2v_{\theta\theta}$ is given by

$$2v_{\theta\theta} = \frac{2N_{\theta\theta}}{J_{\theta\theta} + \Delta J_{\theta\theta}}, \quad (43)$$

where $2N_{\theta\theta}$ is the pitch damping coefficient, $J_{\theta\theta}$ is the pitch moment of inertia, and $\Delta J_{\theta\theta}$ is the added pitch moment of inertia.

The natural circular frequency of the pitch motion is given by

$$n_\theta = \sqrt{\frac{DH_\theta}{J_{\theta\theta} + \Delta J_{\theta\theta}}}, \quad (44)$$

where H_θ is the pitch metacentric height. The pitch moment of inertia $J_{\theta\theta}$ can be estimated using the following formula:

$$J_{\theta\theta} = \frac{1}{12}m(L^2 + H^2), \quad (45)$$

where H is the height of the vessel.

The empirical formula for the added pitch moment of inertia $\Delta J_{\theta\theta}$ is given by

$$\Delta J_{\theta\theta} = C_m \cdot \rho \cdot V \cdot L^2, \quad (46)$$

where C_m is an empirical coefficient, typically taken as 0.1.

The empirical formula for the pitch damping coefficient $N_{\theta\theta}$ is given as follows:

$$N_{\theta\theta} = C_d \cdot \rho \cdot V \cdot B \cdot L, \quad (47)$$

where C_d is an empirical coefficient, typically taken as 0.1 for small vessels.

With the formulas for the vessel and transducer motion parameters and the established physical model of vessel motion, the next step is to estimate the angular velocity tensor and the radius vector.

3. The Proposed Method

This section presents an ADCP attitude dynamic error correction method based on angular velocity tensor and radius vector estimation. Using inclinometer data and applying the vessel's roll and pitch motion models, the angular velocity tensor is obtained. The radius vector estimation methods for both shallow and deep water are derived, along with the instantaneous tangential velocity correction formula, and a correction scheme is provided.

We refer to a continuous velocity measurement process that includes multiple ADCP pulse transmissions and receptions (pings) as a single measurement.

The block diagram of this method is shown in Figure 3 and can be briefly summarized as follows: first, the transducers' radius vectors are estimated during a single measurement, and then the estimated radius vectors are applied for velocity correction in subsequent

measurements. In the radius vector estimation process, shown within the red dashed box in the figure, it is assumed that the vessel velocity has either been determined by other methods (such as GPS) or is zero (indicating that the vessel is swaying in place). The physical model of vessel motion is used as a fitting formula, and the nonlinear least-squares method is applied to fit the inclinometer and compass data to obtain the angular velocity tensor. Then, using the estimated angular velocity tensor, the calculated vessel and transducers' motion parameters, and the BT radial velocities measured by the ASC method, a target function is constructed. The nonlinear least-squares method is then applied for parameter estimation, and a global optimization method is employed to find the global optimal solution for the transducers' radius vectors.

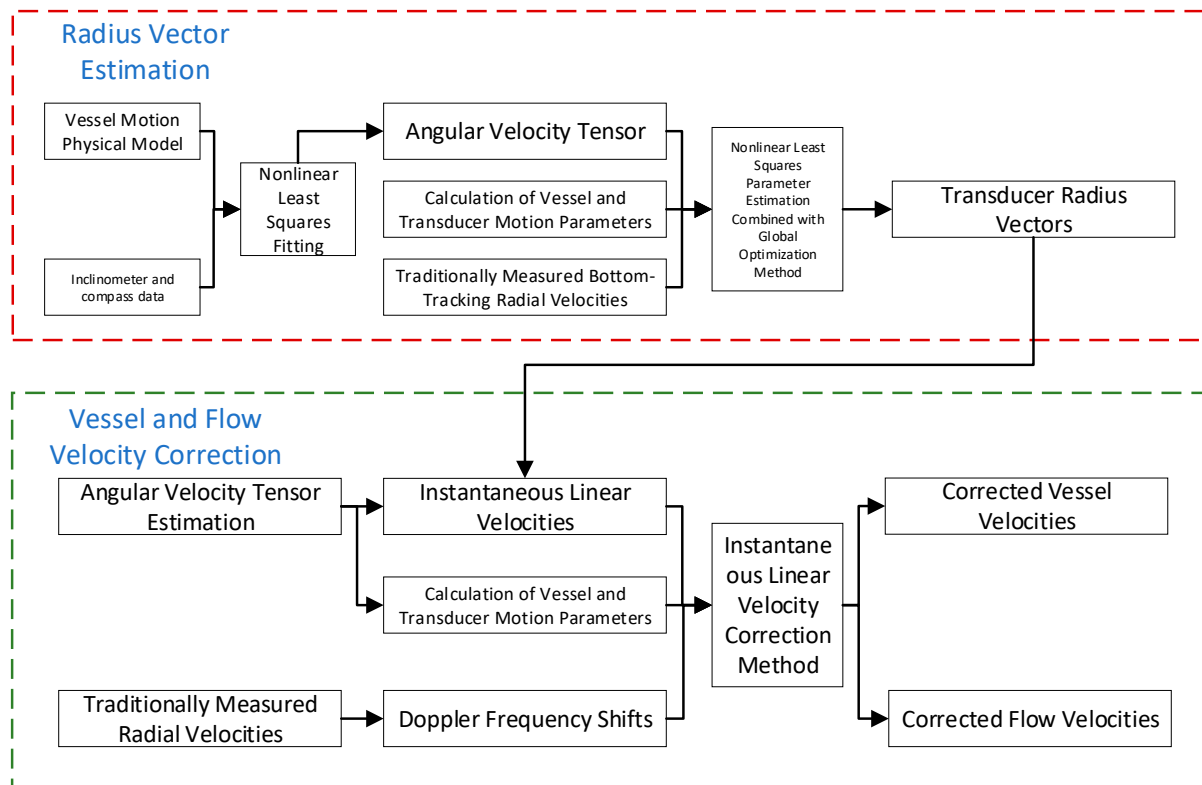


Figure 3. Block diagram illustrating the principle of the proposed ADCP attitude dynamic error correction method, which is based on angular velocity tensor and radius vector estimation.

Within the green dashed box in the figure, representing the measurement of vessel and flow velocities, the instantaneous tangential velocity is derived from the radius vectors estimated in the previous measurement and the angular velocity tensor estimated in the current measurement. The radial velocities measured by the ASC method are then converted into frequency shifts using the Doppler formula. The instantaneous tangential velocity, frequency shifts, and vessel and transducer motion parameters calculated in the current measurement are then used in the instantaneous tangential velocity correction method to ultimately obtain the vessel velocity and flow velocity, which are corrected for the dynamic effects of swaying.

Next, we will derive the methods for estimating the angular velocity tensor and the radius vector, as well as the approach for correcting swaying errors using the instantaneous tangential velocity.

3.1. Estimation of Angular Velocity Tensor

For the roll, pitch, and yaw angle data obtained from the inclinometer and compass, the sampling rate is typically low. This is because the data from all the sensors on a typical

ADCP are bundled and transmitted together, with the data packet update rate being only about 10 Hz, at most, and is often less than 2 Hz. In vessel-installed measurements, the roll frequency of commonly used unmanned monohull vessels is usually around 1 Hz, with the pitch frequency generally being even higher. Thus, the sampling rate is lower than the Nyquist frequency and far below the rate required for data processing tasks such as differentiation.

To address this issue, this study utilizes the physical model of vessel motion. First, the initial values of the parameters in the motion model are calculated using empirical formulas. The measured roll and pitch data are then fitted to the motion model to derive the final formulas for the roll and pitch angles. The detailed steps are outlined below.

As illustrated in the block diagram in Figure 4, which illustrates the method for estimating the angular velocity tensor expression, the roll and pitch motion models from Equations (34) and (41) are used as the fitting formulas. The model parameters calculated from the empirical formulas in Equations (38)–(40) and (45)–(47) serve as the initial guess parameters. Using the nonlinear least-squares method, the roll, pitch, and yaw angles measured by the inclinometer and compass are fitted to obtain the expressions for each angle. Subsequently, the angular velocity tensor expression can be derived using Equation (32).

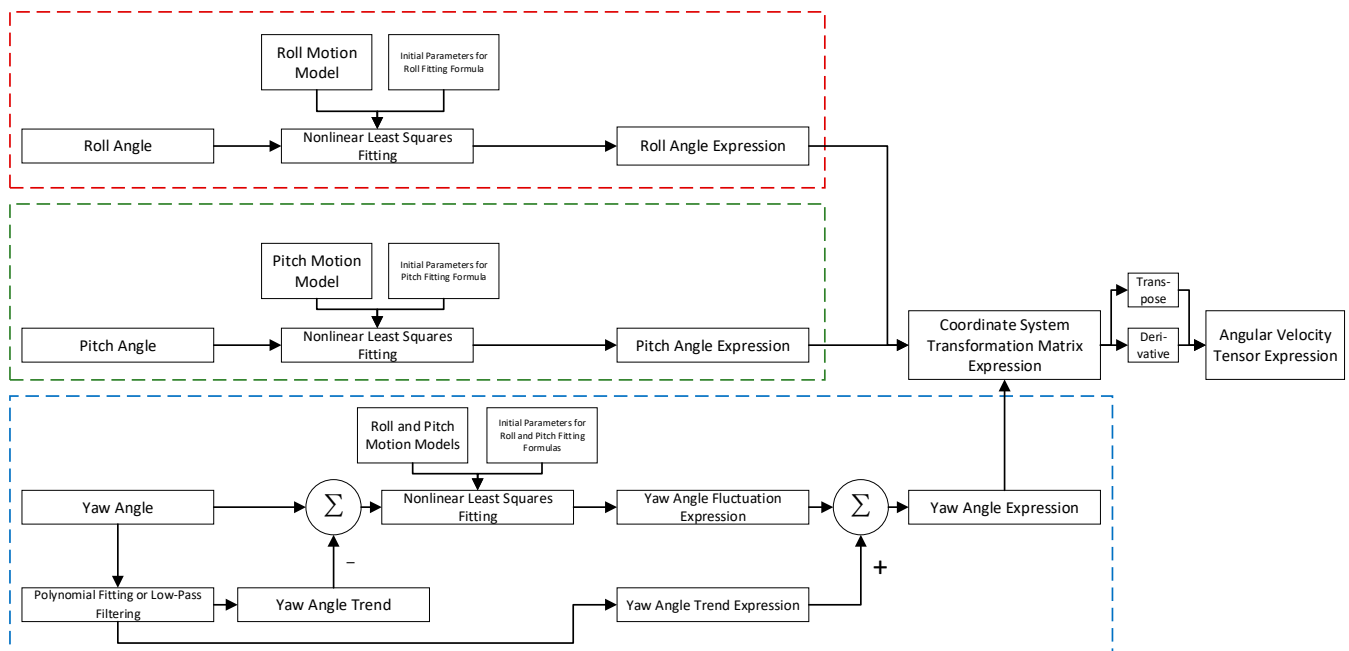


Figure 4. Block diagram for the estimation of angular velocity tensor expression.

Although the yaw angle does not exhibit periodic oscillations, the roll and pitch motions couple with the yaw motion, resulting in a slowly varying, fluctuating yaw angle curve. Therefore, the yaw angle is first detrended using polynomial fitting or low-pass filtering. Then, the roll motion model, combined with the pitch motion model, is used as the fitting formula to fit the detrended yaw angle fluctuations. This process ultimately yields an expression for the yaw angle.

The nonlinear least-squares curve fitting method used in this paper employs the Levenberg–Marquardt algorithm to solve the nonlinear optimization problem. This algorithm dynamically adjusts the damping factor to strike a balance between the Gauss–Newton method and the gradient descent method, thereby achieving fast and stable convergence. It is highly effective for fitting decaying oscillation curves.

In the roll-angle fitting process, the parameters to be estimated are φ_0 , t_{0r} , n_{φ_1} , and $v_{\varphi\varphi}$ from Equation (34), while in the pitch-angle fitting process, the parameters to be estimated are θ_0 , t_{0p} , n_{θ_1} , and $v_{\theta\theta}$ from Equation (41). Let the fitted expressions for the roll, pitch, and

yaw angles be $\hat{\phi}(t)$, $\hat{\theta}(t)$, and $\hat{\psi}(t)$, respectively. Substituting these into Equation (7), the resulting transformation matrix is denoted as $\hat{\Lambda}(t)$. The final expression for the angular velocity tensor is $\hat{\Omega}(t)$. Thus, according to Equation (32), the angular velocity tensor $\hat{\Omega}(t)$ corresponding to $\hat{\Lambda}(t)$ is given by

$$\hat{\Omega}(t) = \dot{\hat{\Lambda}}(t)\hat{\Lambda}^T(t). \quad (48)$$

It is important to note that the purpose of the above processing in this paper is to obtain a usable angular velocity tensor without adding additional hardware devices. If equipment such as a gyroscope or INS provides the roll, pitch, and yaw angle data or angular velocity data with a sufficiently high sampling rate, then those data can be used directly after simple processing.

Once the angular velocity tensor expression is obtained, the radius vector of the transducer's swaying can be estimated.

3.2. Radius Vector Estimation

According to the principles of vessel motion, the angular oscillations of the vessel along the longitudinal, lateral, and vertical axes through the center of gravity G are referred to as the roll, pitch, and yaw, respectively [27]. Accordingly, the transducer's tangential velocity can be determined by the product of the angular velocity tensor and the rotation radius vector. Conversely, if the tangential velocity and angular velocity tensors are known, the swaying radius vector can also be estimated. Based on this principle, when the vessel's velocity (measured by other instruments) is known, the swaying radius vector can be estimated using the BT velocity. Then, through the angular velocity tensor and angles, the transducer's tangential velocity and radial orientation at any given moment can be determined. This allows for the correction of swaying errors using the estimated tangential velocity and radial orientation.

The radius vector is estimated because the transducer's position relative to the vessel's center of gravity is often challenging to determine. If the exact positions of the center of gravity and the transducer installation location are known, the radius vector can be directly calculated.

When the water is relatively shallow, such as for depths within 5 m, the round-trip time of the sound waves is much shorter than the vessel's swaying period. In this case, it can be approximated that the transducer's velocity remains constant throughout the TX and RX of the sound wave, allowing the change in radial angle to be disregarded. However, in deeper waters, where the round-trip time of the sound waves is comparable to the vessel's swaying period, it is necessary to account for the changes in both the transducer's velocity and the radial angle throughout the TX and RX of the sound wave.

The following sections will derive the radius vector formulas for these two cases. Assume that the direction of positive radial velocity is opposite to the transmission direction. Transducers 2, 3, and 4 are selected for the calculations.

A. Radius Vector Estimation Method in Shallow Water

Taking transducer 2 as an example, the radial BT velocity measured at different times, $V_{BTRad2}(t)$, can be expressed as

$$\vec{V}_{T2}(t) \cdot \vec{d}_{T2}(t) = \left[\vec{V}_{T2Sw}(t) + \vec{V}_a(t) \right] \cdot \vec{d}_{T2}(t) = -V_{BTRad2}(t). \quad (49)$$

According to Equation (26), the function of the direction vector of transducer 2 along its acoustic axis, $\vec{d}_{T2}(t)$, with respect to time is given by

$$\vec{d}_{T2}(t) = \Lambda(t)\Lambda_{tb}(\sin \alpha, 0, \cos \alpha)^T. \quad (50)$$

Substituting Equation (48) into Equation (31) gives

$$\vec{V}_{T2Sw}(t) = \hat{\Omega}(t) \vec{r}_{T2}. \quad (51)$$

Thus, substituting Equation (51) into Equation (49) and converting the dot product into matrix multiplication yields

$$\vec{r}_{T2}^T \hat{\Omega}^T(t) \vec{d}_{T2}(t) + \vec{V}_a^T(t) \vec{d}_{T2}(t) = -V_{BTRad2}(t). \quad (52)$$

In Equation (52), \vec{r}_{T2} represents the desired radius vector of transducer 2. Assuming that the positions and orientations of the transducers on the vessel are unknown, the three coordinates of \vec{r}_{T2} are unknown. Additionally, the coordinates of the radius vectors for transducers 3 and 4, \vec{r}_{T3} and \vec{r}_{T4} , are also unknown, resulting in a total of nine unknowns. Since one effective ADCP measurement provides three equations, three effective measurements are required to solve all the radius vectors. Let the times of the three effective measurements be t , t' , and t'' . Let

$$CM_{T2} = \left[\hat{\Omega}^T(t) \vec{d}_{T2}(t), \hat{\Omega}^T(t') \vec{d}_{T2}(t'), \hat{\Omega}^T(t'') \vec{d}_{T2}(t'') \right], \quad (53)$$

$$CM1_{T2} = \left[\vec{V}_a^T(t) \vec{d}_{T2}(t), \vec{V}_a^T(t') \vec{d}_{T2}(t'), \vec{V}_a^T(t'') \vec{d}_{T2}(t'') \right], \quad (54)$$

$$V_{BTRad2All} = [V_{BTRad2}(t), V_{BTRad2}(t'), V_{BTRad2}(t'')]. \quad (55)$$

Thus, CM_{T2} is a 3×3 matrix, and both $CM1_{T2}$ and $V_{BTRad2All}$ are 1×3 vectors. By taking the measurement values of transducer 2 at times t , t' , and t'' as a set, and substituting Equations (53)–(55) into Equation (52), we obtain the matrix equation

$$\vec{r}_{T2}^T CM_{T2} + CM1_{T2} = -V_{BTRad2All}. \quad (56)$$

When CM_{T2} is an invertible matrix, solving this matrix equation yields the radius vector of transducer 2 as

$$\vec{r}_{T2}^T = -(V_{BTRad2All} + CM1_{T2})CM_{T2}^{-1}. \quad (57)$$

Similarly, the radius vectors of transducers 3 and 4 can be obtained as

$$\vec{r}_{Ti}^T = -(V_{BTRadiAll} + CM1_{Ti})CM_{Ti}^{-1}. \quad (58)$$

Here, i takes the values 3 and 4, and in the following Equations (59)–(61), i also takes the values 3 and 4. In the above equation,

$$CM_{Ti} = \left[\hat{\Omega}^T(t) \vec{d}_{Ti}(t), \hat{\Omega}^T(t') \vec{d}_{Ti}(t'), \hat{\Omega}^T(t'') \vec{d}_{Ti}(t'') \right], \quad (59)$$

$$CM1_{Ti} = \left[\vec{V}_a^T(t) \vec{d}_{Ti}(t), \vec{V}_a^T(t') \vec{d}_{Ti}(t'), \vec{V}_a^T(t'') \vec{d}_{Ti}(t'') \right], \quad (60)$$

$$V_{BTRadiAll} = [V_{BTRadi}(t), V_{BTRadi}(t'), V_{BTRadi}(t'')]. \quad (61)$$

Since the angular velocity tensor $\hat{\Omega}(t)$ estimated from inclinometer and compass data has limited accuracy, using estimates at different times tends to result in significant fluctuations in the radius vector, leading to large errors. Therefore, Equations (57) and (58) are generally suitable for situations where $\hat{\Omega}(t)$ is highly accurate. In this paper, where the accuracy of $\hat{\Omega}(t)$ is limited, a local optimization algorithm based on nonlinear least squares can be used to estimate the radius vector. By combining this with a global optimization

method and initiating local optimization from multiple starting points, the chances of finding the global optimal solution are increased.

The specific method involves setting initial values and ranges for the radius vector based on the actual conditions of the vessel and transducers. The objective function for optimization is constructed using Equation (52), and additional constraints are applied based on the Janus array structure of the transducers. Let

$$\vec{r}_T = \left(\vec{r}_{T1}^T, \vec{r}_{T2}^T, \vec{r}_{T3}^T, \vec{r}_{T4}^T \right)^T \quad (62)$$

be the vector composed of the radius vectors to be optimized. The objective function to be minimized is then given as follows:

$$\sum_{i=1}^4 \left[\vec{r}_{Ti}^T \hat{\Omega}^T(t) \vec{d}_{Ti}(t) + \vec{V}_a^T(t) \vec{d}_{Ti}(t) + V_{BTRadi}(t) \right]^2, \quad (63)$$

where time t corresponds to the time points of the data. The following nonlinear inequality constraint conditions are introduced as

$$\begin{cases} \left\| \frac{\vec{r}_{T1} + \vec{r}_{T2} - \vec{r}_{T3} - \vec{r}_{T4}}{2} \right\| \leq \varepsilon_1 \\ \left| \left(\vec{r}_{T1} - \vec{r}_{T2} \right) \cdot \left(\vec{r}_{T3} - \vec{r}_{T4} \right) \right| \leq \varepsilon_2 \\ \left| \left\| \vec{r}_{T1} - \vec{r}_{T2} \right\| - \left\| \vec{r}_{T3} - \vec{r}_{T4} \right\| \right| \leq \varepsilon_3 \end{cases} \quad (64)$$

These three equations correspond to the constraints that ensure that the midpoints of the two diagonal pairs of transducers coincide, the connecting lines are perpendicular, and the distances are equal, thus maintaining the Janus array configuration of the transducers. ε_1 , ε_2 , and ε_3 are small positive values representing the allowable variation range for the left-hand side of the constraint equations.

Therefore, when the accuracy of $\hat{\Omega}(t)$ is limited, the above optimization method can be used to estimate the transducer radius vectors \vec{r}_{T1} , \vec{r}_{T2} , \vec{r}_{T3} , and \vec{r}_{T4} .

B. Radius Vector Estimation Method in Deep Water

According to the relationship between the vessel's radial velocity and the Doppler frequency shift in conventional ADCPs, the measured V_{BTRad2} can be used to obtain the frequency of transducer 2 receiving the bottom echo as follows:

$$f_2 = f_0 \frac{c - V_{BTRad2}}{c + V_{BTRad2}}, \quad (65)$$

where f_0 is the transmission signal frequency, and f_2 is the bottom-echo frequency of transducer 2.

According to Equation (15), the depth of transducer 2 at the time of pulse transmission, $H_{T2}(t_T)$, is given by

$$H_{T2}(t_T) = \vec{T}_2(t_T) \cdot (0, 0, 1)^T + H_O. \quad (66)$$

Thus, the radial distance from transducer 2 to the seabed, denoted as l_2 , is given by

$$l_2 = \frac{H - H_{T2}(t_T)}{\vec{d}_{T2}(t_T) \cdot (0, 0, 1)^T}. \quad (67)$$

Thus, the moment the bottom echo reaches transducer 2, labeled as t_{R2} , is represented by

$$t_{R2} = t_T + \frac{2l_2}{c}. \quad (68)$$

Furthermore, the function of the radial velocity of transducer 2 with respect to time, $V_{TRad2}(t)$, is given by

$$V_{TRad2}(t) = - \left[\vec{V}_a + \vec{V}_{T2Sw}(t) \right] \cdot \vec{d}_{T2}(t). \quad (69)$$

Taking into account the additional tangential velocity and the change in radial direction due to dynamic swaying, the actual expression for f_2 , based on the Doppler formula, should be

$$\begin{aligned} f_2 &= f_0 \frac{c - V_{TRad2}(t_{R2})}{c + V_{TRad2}(t_T)} \\ &= f_0 \frac{c + \left[\vec{V}_a + \vec{V}_{T2Sw}(t_{R2}) \right] \cdot \vec{d}_{T2}(t_{R2})}{c - \left[\vec{V}_a + \vec{V}_{T2Sw}(t_T) \right] \cdot \vec{d}_{T2}(t_T)}. \end{aligned} \quad (70)$$

Here, $\vec{d}_{T2}(t)$ can be obtained from Equation (50).

Thus, substituting Equation (51) into Equation (70), and converting the dot product into matrix multiplication, we obtain

$$\begin{aligned} \vec{r}_{T2}^T \left[f_0 \hat{\Omega}^T(t_{R2}) \vec{d}_{T2}(t_{R2}) + f_2(t_T) \hat{\Omega}^T(t_T) \vec{d}_{T2}(t_T) \right] = \\ - \vec{V}_a^T(t_T) \left[\vec{d}_{T2}(t_{R2}) + \vec{d}_{T2}(t_T) \right] - [f_0 - f_2(t_T)]c. \end{aligned} \quad (71)$$

Let the corresponding times in the other two measurements be denoted as t_T' , t_{R2}' , t_T'' , and t_{R2}'' . Let

$$CM_{T2Dep} = \begin{bmatrix} f_0 \hat{\Omega}^T(t_{R2}) \vec{d}_{T2}(t_{R2}) + f_2(t_T) \hat{\Omega}^T(t_T) \vec{d}_{T2}(t_T), \\ f_0 \hat{\Omega}^T(t_{R2}') \vec{d}_{T2}(t_{R2}') + f_2(t_T') \hat{\Omega}^T(t_T') \vec{d}_{T2}(t_T'), \\ f_0 \hat{\Omega}^T(t_{R2}'') \vec{d}_{T2}(t_{R2}'') + f_2(t_T'') \hat{\Omega}^T(t_T'') \vec{d}_{T2}(t_T'') \end{bmatrix}, \quad (72)$$

$$CM1_{T2Dep} = \begin{bmatrix} -\vec{V}_a^T(t_T) \left[\vec{d}_{T2}(t_{R2}) + \vec{d}_{T2}(t_T) \right] - [f_0 - f_2(t_T)]c, \\ -\vec{V}_a^T(t_T') \left[\vec{d}_{T2}(t_{R2}') + \vec{d}_{T2}(t_T') \right] - [f_0 - f_2(t_T')]c, \\ -\vec{V}_a^T(t_T'') \left[\vec{d}_{T2}(t_{R2}'') + \vec{d}_{T2}(t_T'') \right] - [f_0 - f_2(t_T'')]c \end{bmatrix}. \quad (73)$$

By taking the measurement values of transducer 2 from these three measurements as a set and substituting Equations (72) and (73) into Equation (71), the following matrix equation is obtained:

$$\vec{r}_{T2}^T CM_{T2Dep} = CM1_{T2Dep}. \quad (74)$$

When CM_{T2Dep} is an invertible matrix, solving this matrix equation yields the radius vector of transducer 2:

$$\vec{r}_{T2}^T = CM1_{T2Dep} CM_{T2Dep}^{-1}. \quad (75)$$

Similarly, the radius vectors of transducers 3 and 4 can be obtained:

$$\vec{r}_{Ti}^T = CM1_{TiDep} CM_{TiDep}^{-1}. \quad (76)$$

Here, i takes the values 3 and 4, and in Equations (77) and (78), i also takes the values 3 and 4. In the above equation,

$$CM_{TiDep} = \begin{bmatrix} f_0 \hat{\Omega}^T(t_{Ri}) \vec{d}_{Ti}(t_{Ri}) + f_i(t_T) \hat{\Omega}^T(t_T) \vec{d}_{Ti}(t_T), \\ f_0 \hat{\Omega}^T(t_{Ri}') \vec{d}_{Ti}(t_{Ri}') + f_i(t_{T'}) \hat{\Omega}^T(t_{T'}) \vec{d}_{Ti}(t_{T'}), \\ f_0 \hat{\Omega}^T(t_{Ri}'') \vec{d}_{Ti}(t_{Ri}'') + f_i(t_{T''}) \hat{\Omega}^T(t_{T''}) \vec{d}_{Ti}(t_{T''}) \end{bmatrix}, \quad (77)$$

$$CM1_{TiDcp} = \begin{bmatrix} -\vec{V}_a^T(t_T) \left[\vec{d}_{Ti}(t_{Ri}) + \vec{d}_{Ti}(t_T) \right] - [f_0 - f_i(t_T)]c, \\ -\vec{V}_a^T(t_{T'}) \left[\vec{d}_{Ti}(t_{Ri}') + \vec{d}_{Ti}(t_{T'}) \right] - [f_0 - f_i(t_{T'})]c, \\ -\vec{V}_a^T(t_{T''}) \left[\vec{d}_{Ti}(t_{Ri}'') + \vec{d}_{Ti}(t_{T''}) \right] - [f_0 - f_i(t_{T''})]c \end{bmatrix}. \quad (78)$$

After obtaining the radius vectors of transducers 2, 3, and 4, the corresponding tangential velocities can be determined from Equation (51) as follows:

$$\vec{V}_{T2Sw}(t) = \hat{\Omega}(t) \vec{r}_{T2}, \quad (79)$$

$$\vec{V}_{T3Sw}(t) = \hat{\Omega}(t) \vec{r}_{T3}, \quad (80)$$

$$\vec{V}_{T4Sw}(t) = \hat{\Omega}(t) \vec{r}_{T4}. \quad (81)$$

Similarly, Equations (75) and (76) are generally suitable for situations where $\hat{\Omega}(t)$ is highly accurate. In this paper, where the accuracy of $\hat{\Omega}(t)$ is limited, a local optimization algorithm based on nonlinear least squares can be used to estimate the radius vector. By combining this with a global optimization method and by initiating local optimization from multiple starting points, the chances of finding the global optimal solution are increased.

The specific method is the same as the radius vector estimation method used in shallow water. Let

$$\vec{r}_T = \left(\vec{r}_{T1}^T, \vec{r}_{T2}^T, \vec{r}_{T3}^T, \vec{r}_{T4}^T \right)^T \quad (82)$$

be the vector composed of the radius vectors to be optimized. Based on Equation (71), the objective function to be minimized is given as follows:

$$\sum_{i=1}^4 \left\{ \vec{r}_{Ti}^T \left[f_0 \hat{\Omega}^T(t_{Ri}) \vec{d}_{Ti}(t_{Ri}) + f_i(t_T) \hat{\Omega}^T(t_T) \vec{d}_{Ti}(t_T) \right] + \frac{\vec{V}_a^T(t_T) \left[\vec{d}_{Ti}(t_{Ri}) + \vec{d}_{Ti}(t_T) \right] + [f_0 - f_i(t_T)]c}{\left[f_0 \hat{\Omega}^T(t_{Ri}) \vec{d}_{Ti}(t_{Ri}) + f_i(t_T) \hat{\Omega}^T(t_T) \vec{d}_{Ti}(t_T) \right]} \right\}^2. \quad (83)$$

Here, t corresponds to the time points of the data. The nonlinear inequality constraints to be introduced are the same as those in Equation (64) and will, thus, not be repeated here.

Therefore, when the accuracy of $\hat{\Omega}(t)$ is limited, the above optimization method can be used to estimate the radius vectors \vec{r}_{T1} , \vec{r}_{T2} , \vec{r}_{T3} , and \vec{r}_{T4} in deep-water conditions.

The above method allows for attitude dynamic error correction through software algorithms without modifying the existing ADCP hardware. After estimating the radius vectors and obtaining the transducer's swaying tangential velocity at each moment, the flow velocity and BT velocity are then corrected through the instantaneous tangential velocity correction method described in the next section.

The following section develops the method for correcting errors induced by swaying, utilizing the transducer's swaying tangential velocity, position, and radial direction, which were previously estimated or measured by devices like an INS.

3.3. Correcting Swaying Errors Using Instantaneous Tangential Velocity

Using the coordinate system shown in Figure 1 and considering a single TX and RX process, the conventional ADCP measures the radial BT velocity as $V_{BTRad2Tra}$ and the radial flow velocity at depth H_n as $V_{nRad2Tra}$. The direction for the positive radial velocity is specified as being along the acoustic axis towards the transducer, and all radial velocities are relative to the Earth. Let the navigation velocity (velocity in the equilibrium coordinate system) be \vec{V}_a and the flow velocity at the measured point at depth H_n be \vec{V}_n .

Neglecting the displacement of the transducers during signal TX and RX, we consider the variations in tangential velocity and radial orientation throughout this period. It is assumed that the navigation velocity \vec{V}_a remains constant throughout a single signal TX and RX process.

Thus, according to the relationship between the vessel's radial velocity, flow radial velocity, and Doppler frequency shift in conventional ADCPs, the measured $V_{BTRad2Tra}$ and $V_{nRad2Tra}$ can be used to obtain the corresponding echo frequencies as follows:

$$f_2 = f_0 \frac{c - V_{BTRad2Tra}}{c + V_{BTRad2Tra}}, \quad (84)$$

$$f_{n2} = f_0 \frac{(c + V_{nRad2Tra})(c - V_{BTRad2Tra})}{(c + V_{BTRad2Tra})(c - V_{nRad2Tra})}, \quad (85)$$

where f_0 is the transmission signal frequency, f_2 is the bottom-echo frequency, and f_{n2} is the echo frequency from the water layer at depth H_n .

The distance from transducer 2 to the measurement point at depth H_n , denoted as l_{n2} , is given by

$$l_{n2} = \frac{H_n - H_{T2}(t_T)}{\vec{d}_{T2}(t_T) \cdot (0, 0, 1)^T}. \quad (86)$$

The time at which the echo from the measurement point at depth H_n reaches transducer 2, denoted as t_{Rn2} , is given by

$$t_{Rn2} = t_T + \frac{2l_{n2}}{c}. \quad (87)$$

Taking into account the additional tangential velocity and changes in the radial direction due to dynamic swaying, the actual expression for f_{n2} based on the Doppler formula is given by

$$\begin{aligned} f_{n2} &= f_0 \frac{c - \vec{V}_n \cdot \vec{d}_{T2}(t_T)}{c + V_{TRad2}(t_T)} \frac{c - V_{TRad2}(t_{Rn2})}{c + \vec{V}_n \cdot \vec{d}_{T2}(t_{Rn2})} \\ &= f_0 \frac{c - \vec{V}_n \cdot \vec{d}_{T2}(t_T)}{c - [\vec{V}_a + \vec{V}_{T2Sw}(t_T)] \cdot \vec{d}_{T2}(t_T)} \frac{c + [\vec{V}_a + \vec{V}_{T2Sw}(t_{Rn2})] \cdot \vec{d}_{T2}(t_{Rn2})}{c + \vec{V}_n \cdot \vec{d}_{T2}(t_{Rn2})}. \end{aligned} \quad (88)$$

Here, $\vec{d}_{T2}(t)$ and $\vec{V}_{T2Sw}(t)$ can be obtained from Equations (50) and (79), respectively. Thus, Equation (70) is an equation in terms of \vec{V}_a , and Equation (88) is an equation in terms of both \vec{V}_a and \vec{V}_n . Rewriting the dot product in Equation (70) as a matrix multiplication and simplifying, we obtain the following:

$$\begin{aligned} \vec{V}_a^T \left[f_0 \vec{d}_{T2}(t_{R2}) + f_2 \vec{d}_{T2}(t_T) \right] &= \\ -f_0 \vec{V}_{T2Sw}^T(t_{R2}) \vec{d}_{T2}(t_{R2}) - f_2 \vec{V}_{T2Sw}^T(t_T) \vec{d}_{T2}(t_T) - (f_0 - f_2)c. \end{aligned} \quad (89)$$

Similarly, for transducers 3 and 4, each yields an equation like Equation (89) in terms of \vec{V}_a . By combining these three equations into a system of equations, \vec{V}_a can be solved. To improve clarity and to facilitate calculations, a coefficient matrix is constructed, resulting in an invertible matrix equation. The method is as follows:

Let

$$CM_{Va} = \left[f_0 \vec{d}_{T2}(t_{R2}) + f_2 \vec{d}_{T2}(t_T), f_0 \vec{d}_{T3}(t_{R3}) + f_3 \vec{d}_{T3}(t_T), f_0 \vec{d}_{T4}(t_{R4}) + f_4 \vec{d}_{T4}(t_T) \right], \quad (90)$$

$$CM1_{Va} = \left[\vec{V}_{T2Sw}^T(t_{R2}) \vec{d}_{T2}(t_{R2}), \vec{V}_{T3Sw}^T(t_{R3}) \vec{d}_{T3}(t_{R3}), \vec{V}_{T4Sw}^T(t_{R4}) \vec{d}_{T4}(t_{R4}) \right], \quad (91)$$

$$CM2_{Va} = \left[f_2 \vec{V}_{T2Sw}^T(t_T) \vec{d}_{T2}(t_T), f_3 \vec{V}_{T3Sw}^T(t_T) \vec{d}_{T3}(t_T), f_4 \vec{V}_{T4Sw}^T(t_T) \vec{d}_{T4}(t_T) \right], \quad (92)$$

$$CM3_{Va} = [(f_0 - f_2)c, (f_0 - f_3)c, (f_0 - f_4)c]. \quad (93)$$

The solutions for t_{R3} and t_{R4} are similar to the solution for t_{R2} and will not be elaborated here.

Thus, the solution for \vec{V}_a is given by

$$\vec{V}_a^T = -(f_0 CM1_{Va} + CM2_{Va} + CM3_{Va}) CM_{Va}^{-1}. \quad (94)$$

Similarly, Equation (88) can be simplified as

$$\vec{V}_n^T \left\{ f_{n2}[c + V_{TRad2}(t_T)] \vec{d}_{T2}(t_{Rn2}) + f_0[c - V_{TRad2}(t_{Rn2})] \vec{d}_{T2}(t_T) \right\} = \{ f_0[c - V_{TRad2}(t_{Rn2})] - f_{n2}[c + V_{TRad2}(t_T)] \} c. \quad (95)$$

Substituting the obtained \vec{V}_a into Equation (95) results in an equation for \vec{V}_n . Similarly, for transducers 3 and 4, each yields an equation like Equation (95) in terms of \vec{V}_n . By combining these three equations into a system of equations, \vec{V}_n can be solved. As with the previous case, a coefficient matrix is constructed, resulting in an invertible matrix equation. The solution is as follows:

Let

$$CM_{Vn} = \left\{ \begin{array}{l} f_{n2}[c + V_{TRad2}(t_T)] \vec{d}_{T2}(t_{Rn2}) + f_0[c - V_{TRad2}(t_{Rn2})] \vec{d}_{T2}(t_T), \\ f_{n3}[c + V_{TRad3}(t_T)] \vec{d}_{T3}(t_{Rn3}) + f_0[c - V_{TRad3}(t_{Rn3})] \vec{d}_{T3}(t_T), \\ f_{n4}[c + V_{TRad4}(t_T)] \vec{d}_{T4}(t_{Rn4}) + f_0[c - V_{TRad4}(t_{Rn4})] \vec{d}_{T4}(t_T) \end{array} \right\}, \quad (96)$$

$$CM1_{Vn} = \left\{ \begin{array}{l} f_0[c - V_{TRad2}(t_{Rn2})] - f_{n2}[c + V_{TRad2}(t_T)], \\ f_0[c - V_{TRad3}(t_{Rn3})] - f_{n3}[c + V_{TRad3}(t_T)], \\ f_0[c - V_{TRad4}(t_{Rn4})] - f_{n4}[c + V_{TRad4}(t_T)] \end{array} \right\}. \quad (97)$$

The solutions for t_{Rn3} and t_{Rn4} are similar to the solution for t_{Rn2} and will not be elaborated here.

Thus, the solution for \vec{V}_n is given by

$$\vec{V}_n^T = CM1_{Vn} CM_{Vn}^{-1}. \quad (98)$$

Therefore, Equations (94) and (98) represent the corrected the vessel and flow velocities using the ADC method to account for the platform's dynamic swaying effects.

This flow velocity measurement method fully utilizes the existing ADCP's inclinometer and electronic compass data and the physical characteristics of the surface vessel's swaying.

By processing only the data already measured by the ADCP, it can correct for attitude dynamic errors without the need for additional equipment.

4. Water Pool Experiments

To validate the effectiveness of the proposed method—encompassing angular velocity tensor estimation, radius vector estimation, and instantaneous tangential velocity correction—velocity measurement experiments were carried out in the anechoic pool at Southeast University. The experiments involved a small ADCP-equipped boat, first performing stationary free-swaying and then moving while freely swaying. These tests validated the effectiveness of correcting errors from the attitude dynamics in vessel velocity measurements in shallow water.

4.1. Experimental Setup

The experiment utilized the RiverRay ADCP from Teledyne RD Instruments (TRDI), which can automatically switch between broadband and pulse-coherent modes. This ADCP has a BT velocity measurement range of ± 9.5 m/s and a BT depth range of 0.4 to 100 m. It employs a planar phased-array transducer with four beams, each at a 30° angle. During the experiment, the radial velocity, inclinometer, and compass data collected by the RiverRay ADCP were exported via the WinRiver II software (Version 2.17) for further processing. Data packets from the RiverRay ADCP were sent to the computer at intervals ranging from 0.64 to 0.95 s. The boat's actual velocity was determined using motion tracking from video footage. Figure 3 illustrates the positive directions for the roll, pitch, and yaw angles; the roll and pitch are zeroed when the boat is level, and the yaw angle is zero when the bow is oriented due north. The ADCP was mounted on a small boat measuring 0.96 m in length, 0.2 m in width, and 0.18 m in height, with a total mass of 18 kg, including the ADCP.

The schematic diagram of the experimental setup is presented in Figure 5. The pool is square, measuring 8 m in length, 5 m in width, and 5 m in depth. The four beams of the ADCP transducer (1, 2, 3, 4) are positioned in an “X” configuration, as shown in the figure. To reduce the noise caused by potential multiple reflections of sound waves from the water's surface, anechoic covers were placed over other parts of the pool, as shown in the figure. A photograph of the actual transducer is shown in Figure 6.

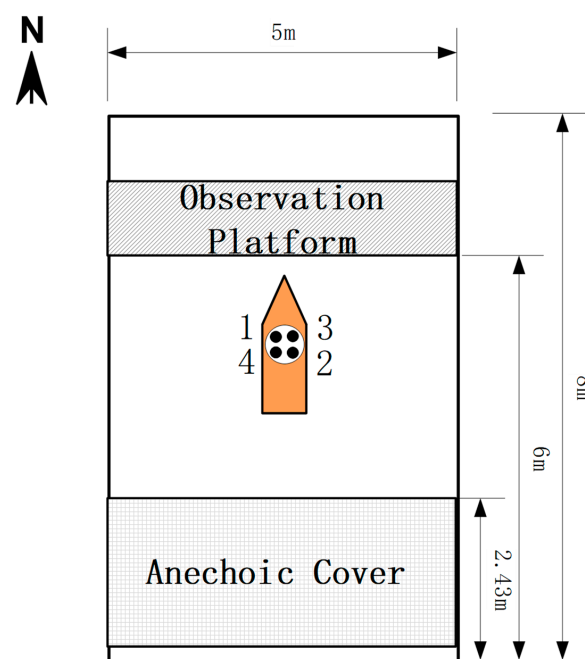


Figure 5. Schematic diagram of the pool experiment.



Figure 6. The RiverRay ADCP transducer.

The actual experimental setup is shown in Figure 7. In Figure 7a, the method of pulling the small boat with a rope is used to move it. The method shown in Figure 7b is used to induce roll motion in the boat.

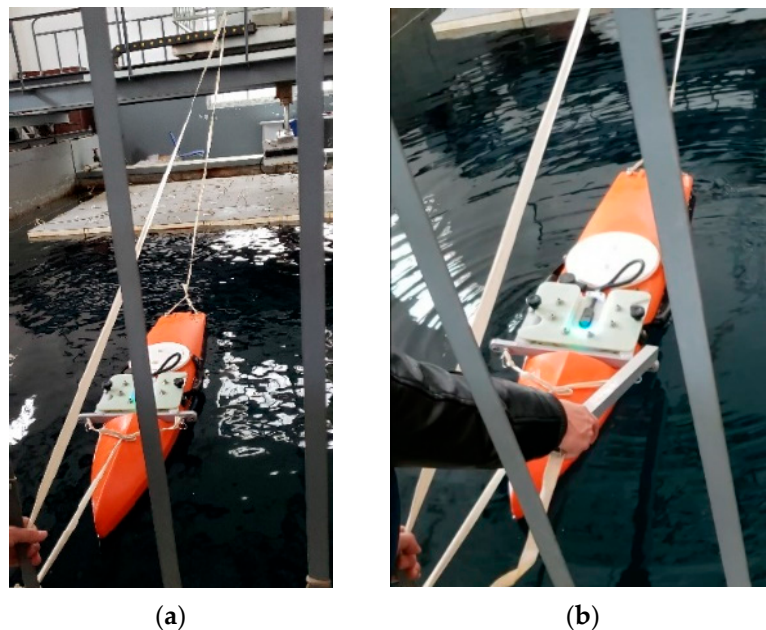


Figure 7. Pool experiment setup diagram: (a) approach for propelling the boat; (b) approach for generating roll motion in the boat.

To estimate the radius vector and to perform attitude dynamic error correction using the radius vector, three measurements were taken with the ADCP during the experiment, resulting in three sets of data. The measurement used for the radius vector estimation is referred to as Measurement 0, the stationary free-swaying measurement as Measurement 1, and the moving free-swaying measurement as Measurement 2. The specific results of these three measurements are presented below.

4.2. Experimental Results and Analysis

A. Radius Vector Estimation Measurement

Using the approach outlined in the preceding section, the transducer's radius vector is initially estimated from a single measurement. The boat was made to sway in place in still

water, and data were collected for the BT radial velocities of the four beams, along with the roll, pitch, and yaw angle measurements. This dataset was then used for the radius vector estimation. First, Equation (34), Equation (41), and their sum are individually used as fitting formulas to fit the roll, pitch, and yaw data from this radius vector estimation measurement, with the aim of determining the angular velocity tensor.

As shown in Tables 1–3, the initial guesses and estimated results of the parameters for the roll, yaw, and pitch motion models during the radius vector estimation measurement are provided. The initial guesses are the starting values used for nonlinear least-squares fitting iterations, which are derived from the empirical formulas for the parameters in Equations (38)–(40) and (45)–(47). From the estimated values of \hat{n}_{φ_1} and \hat{n}_{ψ_1} , it can be seen that the approximate frequencies of the roll and yaw are 1.03 Hz, and the initial times \hat{t}_{0r} and \hat{t}_{0y} are almost identical. It is clear that since the pitch angle is very small, the yaw angle fluctuates with the roll angle.

Table 1. Initial guesses and estimated results of the roll parameters.

Parameters	$\hat{\varphi}_0$ (rad)	\hat{t}_{0r} (s)	\hat{n}_{φ_1} (rad/s)	$\hat{v}_{\varphi\varphi}$ (s ^{−1})	RSS (rad ²)
Initial guess	0.2	0	6.3192	0.0572	-
Estimated value	0.2457	−0.0493	6.1096	0.1123	0.0139

Table 2. Initial guesses and estimated results of the yaw parameters.

Parameters	$\hat{\psi}_0$ (rad)	\hat{t}_{0y} (s)	\hat{n}_{ψ_1} (rad/s)	$\hat{v}_{\psi\psi}$ (s ^{−1})	RSS (rad ²)
Initial guess	−0.1	0	6.3192	0.0572	-
Estimated value	−0.1391	−0.0491	6.1095	0.1365	0.0046

Table 3. Initial guesses and estimated results of the pitch parameters.

Parameters	$\hat{\theta}_0$ (rad)	\hat{t}_{0p} (s)	\hat{n}_{θ_1} (rad/s)	$\hat{v}_{\theta\theta}$ (s ^{−1})	RSS (rad ²)
Initial guess	0.2	0	4.7595	0.6498	-
Estimated value	0.2457	−0.3451	4.2850	0.8908	4.4716×10^{-5}

Figure 8 below shows the corresponding fitting results for the roll, yaw, and pitch angles. It can be seen from the figure that the motion in this measurement is primarily dominated by the roll, with the yaw angle fluctuating along with the roll angle while also exhibiting a slow-changing trend. The pitch angle shows very little variation during this measurement, with values distributed around a bias. The fitted curve closely aligns with nearly all the original data points, with only a few points showing slight deviations from the curve, indicating that the fitting results meet the requirements for the subsequent radius vector estimation.

By substituting the parameters estimated from Table 1 into Equation (34), the parameters estimated from Table 2 into Equation (34) with the trend added, and the parameters estimated from Table 3 into Equation (41), expressions for the roll, yaw, and pitch angles can be obtained. These expressions are then substituted into Equation (48) to derive the angular velocity tensor expression. Next, the angular velocity tensor and the calculated vessel and transducer motion parameters are substituted into Equation (63) to obtain the objective function. Considering the constraints in Equation (64), the radius vectors are estimated using a nonlinear least-squares local optimization algorithm combined with a global optimization method.

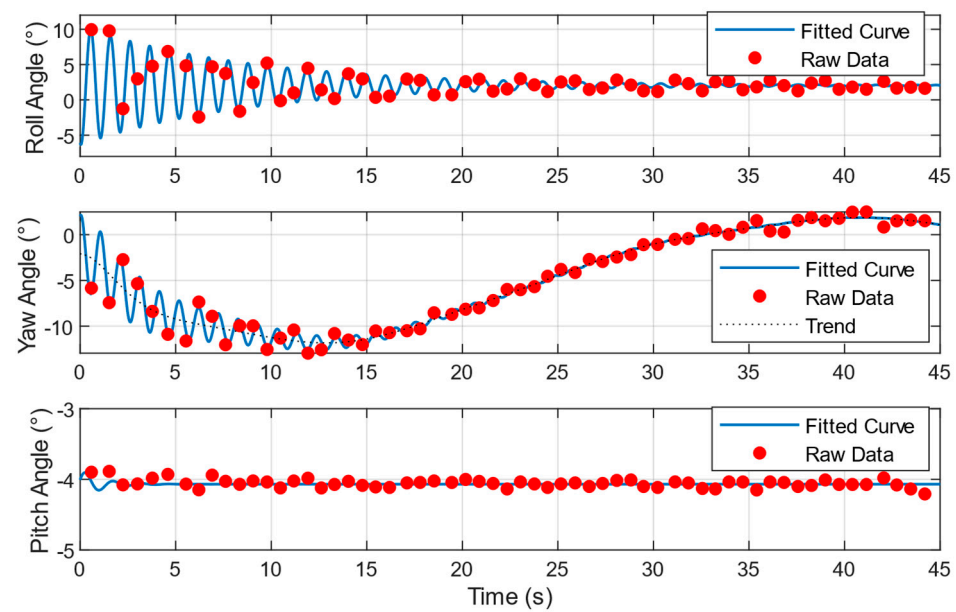


Figure 8. Fitting results of the roll, yaw, and pitch angles in the radius vector estimation measurement.

The estimated radius vectors for transducers 1, 2, 3, and 4 are shown in Table 4. The positions of the radius vectors within the coordinate system are illustrated in Figure 9, where Figure 9b provides a top-down view of the radius vectors. From the figure, it can be seen that the four transducers are essentially arranged at the four corners of a square, conforming to the shape of the Janus array. The side length of the square formed by the four transducers is approximately 2 cm, and the projection of the rotation center (the vessel's center of gravity; G) also lies within this square. The z-coordinate of the radius vectors is approximately 14 cm, which is relatively large compared with the x and y coordinates, and they are close in magnitude to that of the radius vectors. This suggests that in the experiment, the transducers' tangential velocity is primarily affected by their vertical distance from the vessel's center of gravity.

Table 4. Estimated transducer radius vectors.

Parameters	\vec{r}_{T1} (m)	\vec{r}_{T2} (m)	\vec{r}_{T3} (m)	\vec{r}_{T4} (m)	RSS (m ² /s ²)
Radius vector coordinates	$\begin{pmatrix} 0.0107 \\ -0.0112 \\ 0.1385 \end{pmatrix}$	$\begin{pmatrix} -0.0101 \\ 0.0102 \\ 0.1393 \end{pmatrix}$	$\begin{pmatrix} 0.0110 \\ 0.0100 \\ 0.1398 \end{pmatrix}$	$\begin{pmatrix} -0.0095 \\ -0.0102 \\ 0.1393 \end{pmatrix}$	0.0054
Radius vector magnitude	0.1393	0.1401	0.1406	0.1400	-

To visually validate the accuracy of the radius vector estimation, Figure 10 shows a comparison between the fitted curves, generated by substituting the estimated radius vectors back into Equation (52), and the original BT radial velocity data. As can be seen from the figure, the fitted curves pass through most of the original data points, indicating that the fitting performance is good.

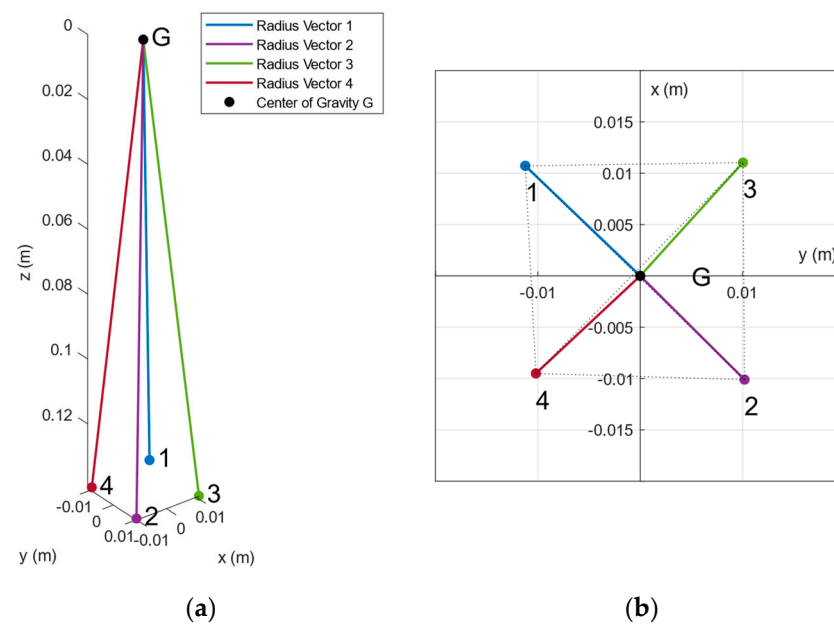


Figure 9. Transducer radius vector diagram. (a) Three-dimensional view of the radius vectors. (b) Top-down view of the radius vectors.

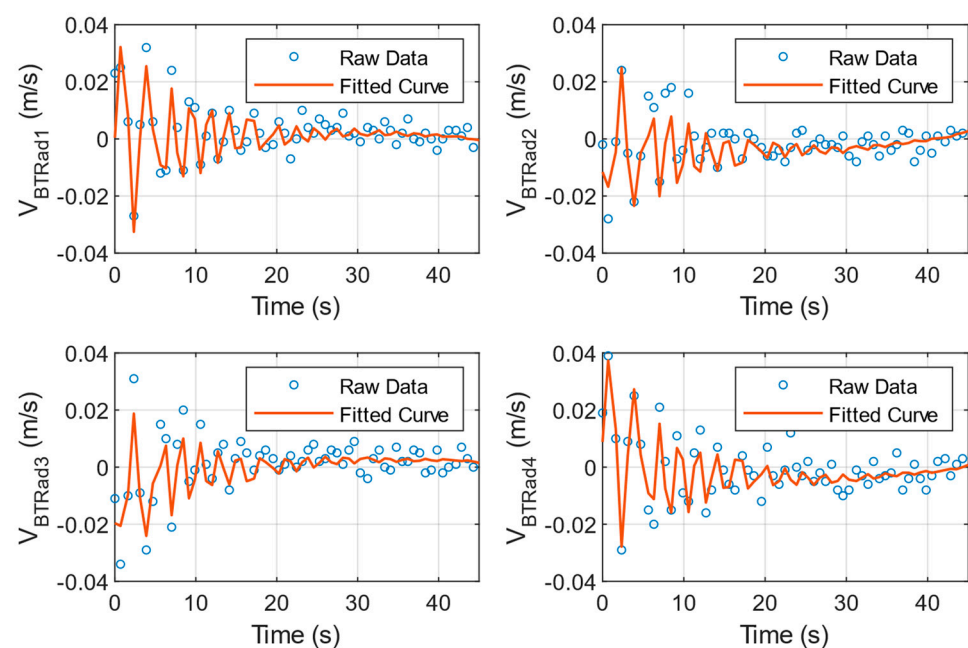


Figure 10. The estimated radius vectors are used to fit the BT (bottom-tracking) radial velocities in this measurement to validate the accuracy of the estimation.

B. Measurement 1

In the previous measurement, the radius vectors of the four transducers were estimated. These radius vectors can now be used in subsequent measurements to correct for errors due to attitude dynamics in the vessel's velocity. First, the vessel's stationary free-swaying motion will be corrected in this measurement; then, in Measurement 2, the vessel's free-swaying motion while moving will be corrected.

In this measurement, the bow of the vessel was oriented westward while it performed stationary free-swaying motions. The roll, yaw, and pitch data from Measurement 1 were fitted to obtain the corresponding angular velocity tensor. The initial guesses and estimated

results for the roll, yaw, and pitch motion model parameters in Measurement 1 are shown in Tables 5–7, respectively. The initial guesses were derived from the empirical formulas for each parameter (Equations (38)–(40) and (45)–(47)).

Table 5. Initial guesses and estimated results of the roll parameters in Measurement 1.

Parameters	$\hat{\varphi}_0$ (rad)	\hat{t}_{0r} (s)	\hat{n}_{φ_1} (rad/s)	$\hat{v}_{\varphi\varphi}$ (s ^{−1})	RSS (rad ²)
Initial guess	−0.2	0	6.3192	0.0572	−
Estimated value	−0.2187	1.1403	6.1919	0.1441	0.0025

Table 6. Initial guesses and estimated results of the yaw parameters in Measurement 1.

Parameters	$\hat{\psi}_0$ (rad)	\hat{t}_{0r} (s)	\hat{n}_{φ_1} (rad/s)	$\hat{v}_{\varphi\varphi}$ (s ^{−1})	RSS (rad ²)
Initial guess	0.1	0	6.3192	0.0572	−
Estimated value	0.1270	1.1403	6.1919	0.5757	0.0014

Table 7. Initial guesses and estimated results of the pitch parameters in Measurement 1.

Parameters	$\hat{\theta}_0$ (rad)	\hat{t}_{0p} (s)	\hat{n}_{θ_1} (rad/s)	$\hat{v}_{\theta\theta}$ (s ^{−1})	RSS (rad ²)
Initial guess	0.02	0	4.7595	0.6498	−
Estimated value	0.0022	0.0189	4.7700	0.2952	2.6663×10^{-5}

Figure 11 shows the corresponding fitting results for the roll, yaw, and pitch angles. From the figure, it can be observed that this measurement is also primarily dominated by the roll motion, with the yaw angle fluctuating along with the roll angle while exhibiting a slow-changing trend. The pitch angle shows very little variation during this measurement, with values distributed around the bias.

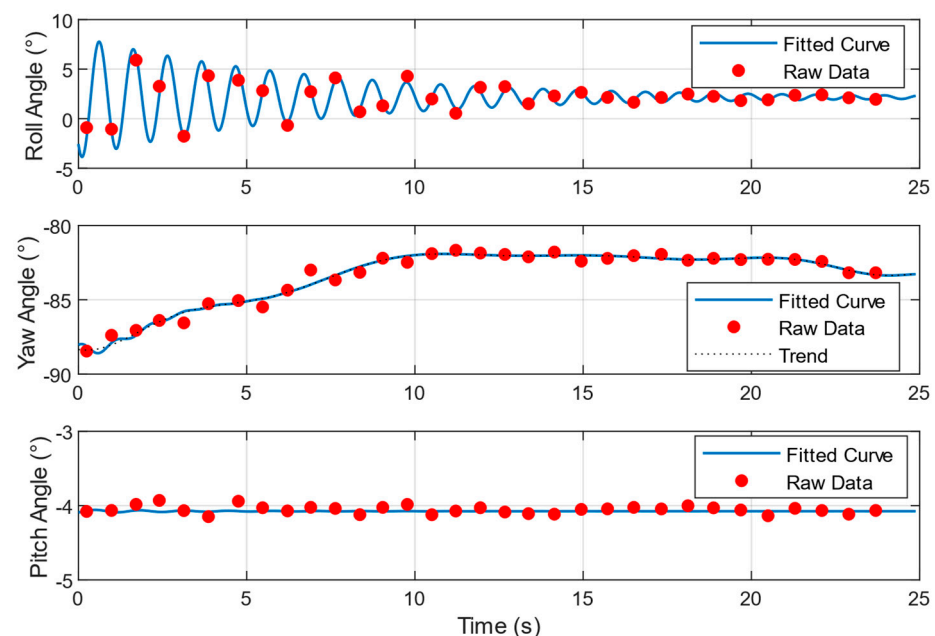


Figure 11. Fitting results of the roll, yaw, and pitch angles in Measurement 1.

After estimating the parameters of the motion physical model, the method for obtaining the angular velocity tensor expression is the same as in the radius vector estimation measurement.

Using the roll, yaw, and pitch angles and the angular velocity tensor expressions obtained above, the vessel and transducer motion parameters for Measurement 1 can be

calculated. Then, using Equation (94), the swaying errors can be corrected. The angular velocity magnitude and vessel velocity derived using the ASC method are shown in Figure 12, where the angular velocity magnitude is the norm of the angular velocity vector, calculated using Equation (33). The comparison in Figure 12 reveals that fluctuations in the vessel velocity measured by the ASC method closely align with the angular velocity magnitude, suggesting that the vessel's swaying significantly affects the vessel velocity measured with this method.

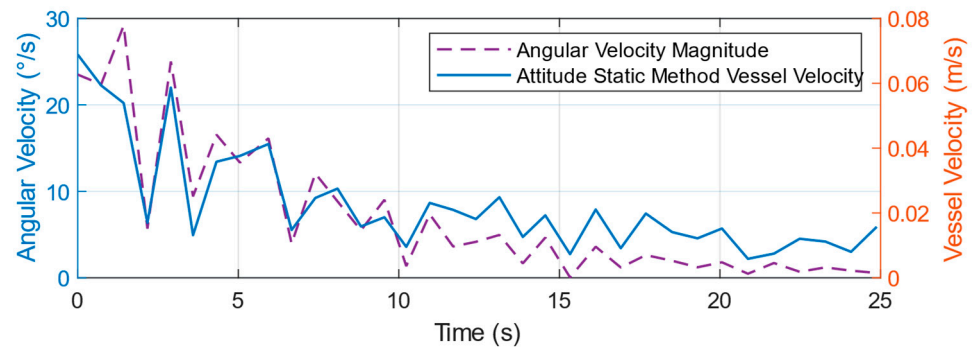


Figure 12. Measurement 1 vessel angular velocity magnitude and the ASC method vessel velocity.

Figure 13 presents a comparison of vessel velocity magnitudes between the ASC method and the proposed method. The figure shows a significant reduction in velocity fluctuations when using the proposed method. Despite attempts to keep the vessel stationary while allowing free-swaying during the measurement, minor movement occurred, as indicated by the black dashed line. Examining the curves, it is evident that the velocity magnitude curve from the proposed method aligns more closely with the actual vessel velocity magnitude, particularly when the angular velocity magnitude is high. In such instances, the velocity magnitude from the ASC method is notably higher than that of the proposed method and the actual velocity magnitude.

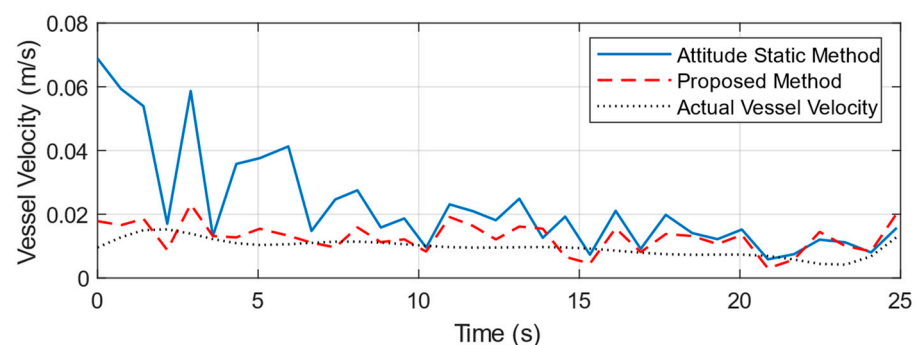


Figure 13. Vessel velocities in Measurement 1 obtained with the ASC method and the proposed method.

Figure 14 shows a comparison of the vessel velocity direction between the ASC method and the proposed method. The directions of the vessel velocity in both methods reflect the scenario of the vessel swaying in place, with its bow facing west. The black dashed arrows, indicating the vessel's actual velocity direction, along with the velocity magnitude shown in Figure 13, reveal that the vessel was moving at a very low speed toward the southeast. The blue arrows in the figure indicate that the vessel velocity direction obtained from the ASC method oscillated between the north and south directions, with the amplitude of these oscillations gradually decreasing over time. This corresponds to the scenario of the vessel primarily rolling from side to side with its bow facing west, as reflected in Figure 11. The red dashed arrows represent the velocity direction obtained from the

proposed method. In comparison with the ASC method, the proposed method's vessel velocity direction is significantly less influenced by vessel swaying and aligns more closely with the actual direction.

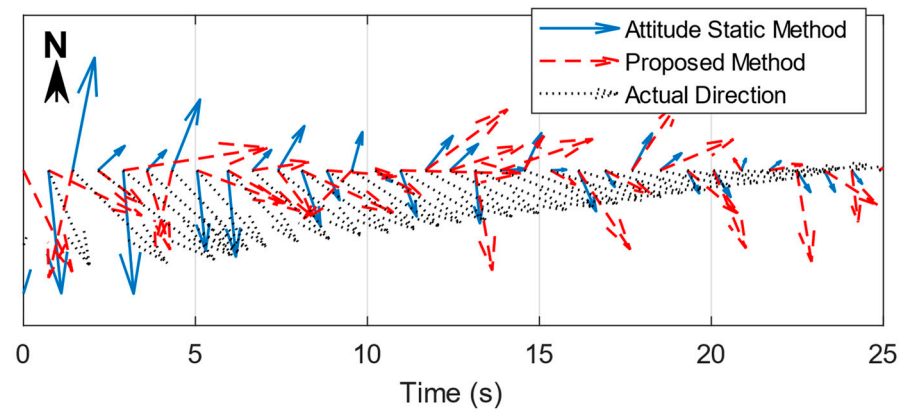


Figure 14. Vessel velocity directions in Measurement 1 obtained with the ASC method and the proposed method.

Subsequently, the mean, standard deviation (SD), relative standard deviation (RSD), mean absolute error (MAE), mean relative error (MRE), and error SD for vessel velocities obtained from the ASC method and the proposed method and from the actual vessel velocity magnitudes were calculated. The vessel displacement was determined by integrating these vessel velocities, after which the magnitude of the displacement and other related metrics were computed. Table 8 presents these results, where RSD denotes the relative standard deviation, calculated as the ratio of SD to the mean. Error SD represents the SD of the error, defined as the difference between the observed and actual values. The vessel displacement is determined as the distance from the origin at 0 s to its location at 45 s. Distance error is the difference between the measured and actual vessel displacement, and distance RE is the ratio of this error to the magnitude of the actual displacement.

Table 8. Table showing the Measurement 1 vessel velocity magnitude and vessel displacement statistics.

	Vessel Velocity Magnitude						Vessel Displacement		
	Mean (m/s)	SD (m/s)	RSD (%)	MAE (m/s)	MRE (%)	Error SD (m/s)	Magnitude (m)	Distance Error (m)	Distance RE (%)
ASC method	0.0219	0.0151	68.91	0.0126	124.65	0.0151	0.2214	0.0161	7.54
Proposed method	0.0125	0.0045	35.53	0.0043	50.84	0.0045	0.2099	0.0073	3.4
Actual value	0.0096	0.0026	27.53	0	0	0	0.2134	0	0
Reduction Amount	0.0094	0.0107	33.39	0.0083	73.81	0.0107	-	0.0088	4.13

From Table 8, it can be seen that in this measurement, the actual vessel velocity magnitude had a very small average value of only 0.0096 m/s. The tangential velocity resulting from the swaying motion constitutes a large part of the overall velocity, which substantially impacts the accuracy of the ASC method. As a result, the average and SD of the vessel velocity magnitude obtained with the ASC method are noticeably greater than those of the actual vessel velocity magnitude. By contrast, the proposed method provides average and SD values for the vessel velocity magnitude that are more closely aligned with the actual values.

Since the vessel's motion in this measurement was primarily due to free swaying, with minimal actual translational velocity, the MRE of vessel velocity magnitudes from the ASC method and the proposed method reached 124.65% and 50.84%, respectively, with RSDs of 68.91% and 35.53%. Consequently, in this stationary free-swaying measurement,

the proposed method decreased the MRE and RSD by 73.81% and 33.39%, respectively, in comparison with the ASC method.

In this measurement, while the proposed method greatly improved vessel velocity accuracy, Table 8 indicates that the displacement magnitude obtained by integrating the velocity vectors from both the ASC method and the proposed method differed from the actual displacement magnitude by less than 8 mm, with displacement errors under 2 cm for both methods. With an actual displacement of approximately 21 cm in this measurement, the relative error (RE) in displacement using the proposed method was decreased by only 4.13% compared with the ASC method.

This suggests that although the proposed method significantly enhanced the velocity measurement accuracy, its impact on the displacement measurement was limited. As previously explained, this outcome is due to the physical model of vessel motion: the vessel's free-swaying motion results in the velocity following an exponentially decaying sinusoidal oscillation. When velocity vectors are integrated over time to determine the vessel displacement, the tangential velocities from different phases of the free-swaying motion tend to offset each other. Consequently, the ADC method provides only a modest improvement in displacement accuracy.

The following section will validate the effectiveness of the proposed method for correcting attitude dynamics of vessel velocity during free swaying in shallow water while in motion and compares it with the ASC method.

C. Measurement 2

In Measurement 2, the vessel moves forward while freely swaying. The correction method is the same as in Measurement 1, resulting in the initial guess values and estimated results for the roll, yaw, and pitch motion model parameters shown in Tables 9–11, respectively. Figure 15 displays the corresponding fitting results for the roll, yaw, and pitch angles. From the figure, it can be observed that this measurement is also primarily dominated by the roll motion, with the yaw angle fluctuating with the roll motion while exhibiting a slow-changing trend. The pitch angle shows very little variation during this measurement, with values distributed around the bias.

Table 9. Initial guesses and estimated results of the roll parameters in Measurement 2.

Parameters	$\hat{\varphi}_0(\text{rad})$	$\hat{t}_{0r}(\text{s})$	$\hat{n}_{\varphi_1}(\text{rad/s})$	$\hat{v}_{\varphi\varphi}(\text{s}^{-1})$	RSS (rad^2)
Initial guess	0.2	0	6.3192	0.0572	-
Estimated value	0.3610	−0.0019	6.1153	0.1508	0.0135.

Table 10. Initial guesses and estimated results of the yaw parameters in Measurement 2.

Parameters	$\hat{\psi}_0(\text{rad})$	$\hat{t}_{0y}(\text{s})$	$\hat{n}_{\psi_1}(\text{rad/s})$	$\hat{v}_{\psi\psi}(\text{s}^{-1})$	RSS (rad^2)
Initial guess	−0.2	0	6.3192	0.0572	-
Estimated value	−0.4327	−0.0019	6.1153	0.1365	0.0330.

Table 11. Initial guesses and estimated results of the pitch parameters in Measurement 2.

Parameters	$\hat{\theta}_0(\text{rad})$	$\hat{t}_{0p}(\text{s})$	$\hat{n}_{\theta_1}(\text{rad/s})$	$\hat{v}_{\theta\theta}(\text{s}^{-1})$	RSS (rad^2)
Initial guess	0.02	0	4.7595	0.6498	-
Estimated value	0.0022	0.3468	5.0853	0.1220	3.9702×10^{-4} .

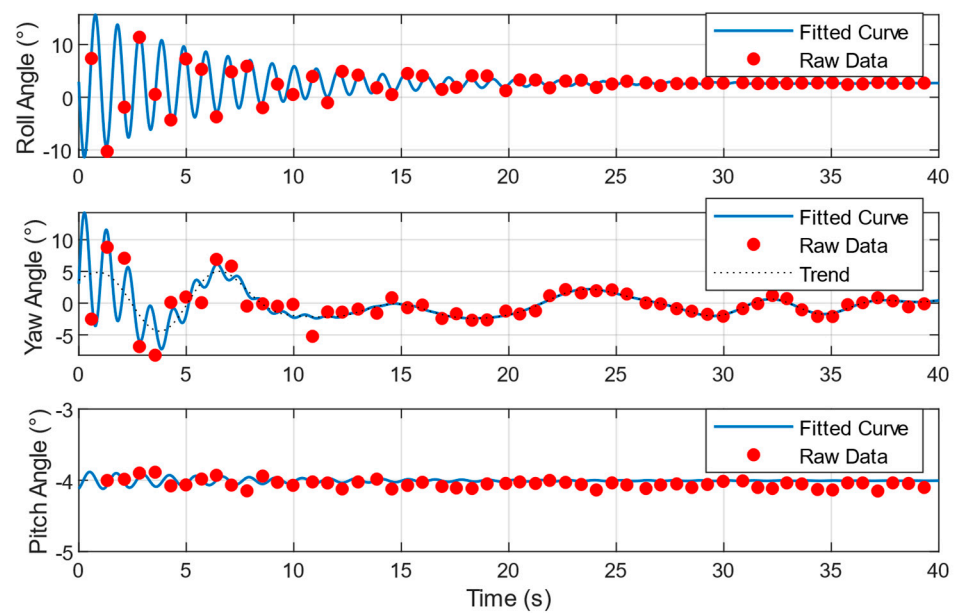


Figure 15. Fitting results of the roll, yaw, and pitch angles in Measurement 2.

After estimating the parameters of the physical motion model, the method for obtaining the angular velocity tensor expression is the same as in the radius vector estimation measurement.

Using the roll, yaw, and pitch angles and the angular velocity tensor expressions obtained above, the vessel and transducer motion parameters for Measurement 2 can be calculated. Then, using Equation (94), the swaying errors can be corrected. The angular velocity magnitude and vessel velocity obtained by applying the ASC method are shown in Figure 16.

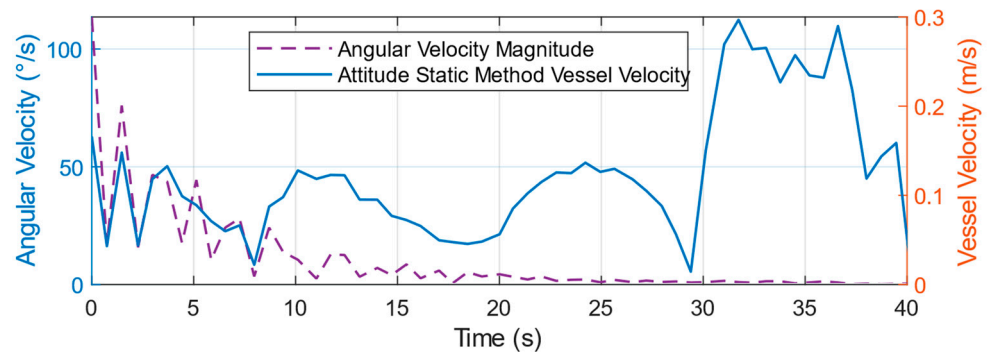


Figure 16. Measurement 2 vessel angular velocity magnitude and the ASC method vessel velocity.

From the comparison in Figure 16, it can be seen that during the first 20 s, the angular velocity magnitude is relatively large, indicating noticeable swaying of the vessel. The angular velocity magnitude then gradually decreases and approaches zero in the last 20 s, indicating that the swaying stops, leaving only translational movement. The fluctuations in the vessel velocity measured by the ASC method correspond closely to the changes in the angular velocity magnitude, indicating that the vessel's swaying had a significant impact on the velocity measured by applying the ASC method during Measurement 2.

Figure 17 presents a comparison of vessel velocity magnitudes between the ASC method and the proposed method. The black vertical dashed line in the figure marks the moment at 29.39 s when the vessel changes its course from moving southward to moving northward. The figure shows that in the first 20 s, when the vessel exhibits noticeable swaying, the velocity fluctuations in the proposed method are considerably smaller than

those in the ASC method and are closer to the actual vessel velocity. As time advances and the rotational angular velocity from swaying gradually decreases, the velocity magnitude curves from both methods converge toward the actual values. This suggests that the proposed method is effective in mitigating the impact of attitude dynamics.

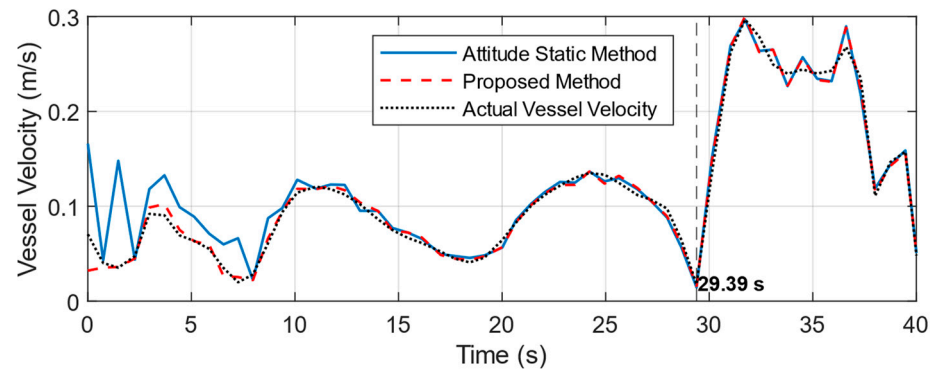


Figure 17. Vessel velocities in Measurement 2 obtained with the ASC method and the proposed method.

Figure 18 presents a comparison of vessel velocity directions between the ASC method and the proposed method. The black dashed arrows in the figure indicate the actual vessel velocity direction, illustrating a scenario where the vessel, with its bow facing north, sways freely, first moving southward and then northward. The blue arrows reveal that during this swaying motion, the vessel velocity direction measured by the ASC method shows not only a southward component but also periodic variations between east and west, indicating a strong influence of the roll motion on the velocity direction. In contrast, the red dashed arrows, which represent the velocity direction derived from the proposed method, display a significantly reduced east–west component, and the angle between the estimated velocity direction and the actual direction is smaller. As the swaying amplitude diminishes over time, the velocity directions measured by both methods gradually align more closely with the actual velocity direction, consistent with the vessel's roll motion while maintaining a northward-facing bow, as shown in Figure 15.

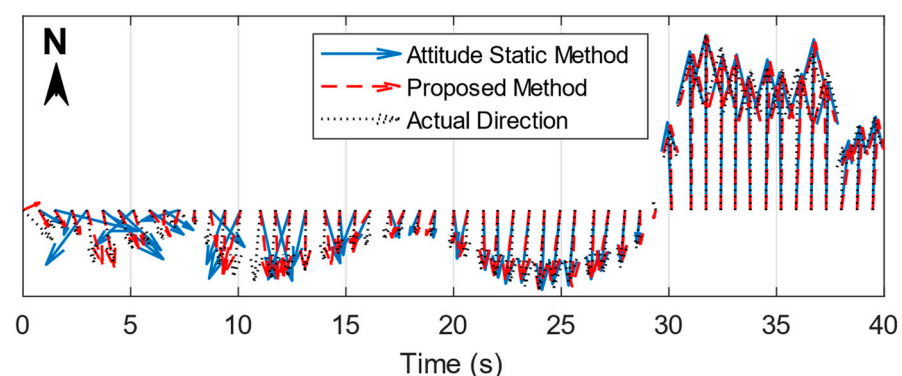


Figure 18. Vessel velocity directions in Measurement 2 obtained with the ASC method and the proposed method.

Next, the vessel velocity magnitude and displacement statistics for the period from 0 to 29.39 s (when the vessel was moving southward) were calculated. For both the ASC method and the proposed method, the mean, MAE, MRE, SD of the error, and RSD of the error were computed for the vessel velocity magnitudes, along with the actual values. By integrating these vessel velocities, the vessel's displacement was derived, and the magnitude of the displacement and the associated metrics were calculated. The results are presented in

Table 12. Vessel displacement is defined as the distance from the origin at 0 s to its location at 45 s. The meanings of the other parameters in Table 12 are the same as those in Table 8.

Table 12. Measurement 2 vessel velocity magnitude and the vessel displacement statistics.

	Vessel Velocity Magnitude					Vessel Displacement		
	Mean (m/s)	MAE (m/s)	MRE (%)	Error SD (m/s)	Error RSD (%)	Magnitude (m)	Distance Error (m)	Distance RE (%)
ASC method	0.0908	0.0138	28.22	0.0234	25.74	2.2243	0.0341	1.51
Proposed method	0.0804	0.0047	7.27	0.0067	8.37	2.2788	0.0205	0.91
Actual value	0.0801	0	0	0	0	2.2584	0	0
Reduction Amount	0.0104	0.0091	20.94	0.0166	17.38	-	0.0136	0.6

Table 12 shows that the mean of the actual vessel velocity magnitude in this measurement is 0.0801 m/s, which is considerably higher than the 0.0096 m/s observed in the prior measurement. Consequently, the share of tangential velocity caused by swaying in the overall velocity is considerably lower. As a result, the differences between the mean vessel velocity magnitudes from the ASC method and the proposed method, relative to the actual value, are minimal, with the proposed method yielding a slightly lower and more accurate magnitude. In this moving free-swaying measurement, the MRE for the vessel velocity magnitude is 28.22% with the ASC method and 7.27% with the proposed method, indicating a decrease of 20.94%. Given the inherent fluctuations in actual vessel velocity, the error SD offers a more reliable assessment of the impact of swaying on the velocity magnitude variability. According to the table, the error SD for the vessel velocity magnitude is 0.0234 m/s with the ASC method and 0.0067 m/s with the proposed method, reflecting a decrease of 0.0166 m/s. The error RSD is 25.74% for the ASC method and 8.37% for the proposed method, representing a decrease of 17.38%. This marked reduction demonstrates that the proposed method effectively mitigates the variability in vessel velocity, thereby significantly enhancing the accuracy and reliability of vessel velocity measurements.

Similarly, because the vessel velocity follows an approximately exponentially decaying sinusoidal oscillation, a significant portion of the tangential velocity cancels out during integration of the velocity vectors. Consequently, the ADC method provides limited improvement in displacement accuracy in this measurement. Table 12 shows that the displacement magnitude obtained through integration of the velocity vectors in both the ASC method and the proposed method deviates from the actual displacement magnitude by less than 4 cm, with the distance errors between the measured and actual displacements for both methods also under 4 cm. With an actual displacement of 2.2584 m in this measurement, the proposed method achieved only a 0.6% reduction in the distance RE compared with the ASC method, indicating a limited improvement in the displacement measurement accuracy.

4.3. Experiment Summary

In this experiment, the transducer radius vectors were first estimated through the stationary free-swaying radius vector estimation measurement (Measurement 0). The estimated radius vectors were subsequently used to correct the vessel velocity in Measurements 1 and 2. The results showed that estimating attitude angles and angular velocity tensors through the combination of the physical model of vessel motion with the nonlinear least-squares method was effective for both the radius vector estimation and the instantaneous tangential velocity correction. The good fitting results for the back-substitution of the radius vectors into the BT radial velocities in Measurement 0, as well as the successful correction of vessel velocity swaying errors using the estimated angular velocity tensors and radius vectors in Measurements 1 and 2, further validate the effectiveness of the angular velocity tensor and radius vector estimation methods. The experiment only verified the effectiveness of the attitude dynamic error correction for vessel velocity during stationary and moving free-swaying conditions in shallow water.

The final results indicate that for Measurement 1, the MREs in vessel velocity using the ASC method and the proposed method were 124.65% and 50.84%, respectively, reflecting a decrease of 73.81%. The RSDs were 68.91% and 35.53%, representing a decrease of 33.39%. In Measurement 2, the MREs were 28.22% for the ASC method and 7.27% for the proposed method, representing a decrease of 20.94%. The RSDs of the errors were 25.74% and 8.37%, respectively, reflecting a decrease of 17.38%. These results demonstrate that the proposed method significantly decreases both the error and variability in vessel velocity, substantially enhancing the velocity accuracy and effectively correcting attitude dynamic errors.

In Measurement 1, the relative distance errors between the displacement derived using the ASC method and the actual displacement and between the displacement obtained using the proposed method and the actual displacement were 7.54% and 3.4%, respectively, marking a reduction of 4.13%. For Measurement 2, the relative distance errors were 1.51% for the ASC method and 0.91% for the proposed method, reflecting a reduction of 0.6%. Thus, the enhancement in displacement measurement accuracy achieved by the proposed method remains limited.

5. Discussion

The physical model of vessel motion used in this paper is based on the assumption of free-swaying motion. In cases of forced swaying or when the vessel is influenced by waves, although the nonlinear least-squares method can extend the applicability of the proposed method to some extent, adjustments to the physical model may be required. The proposed method, although not requiring additional equipment, includes the steps of estimating the radius vector, estimating the angular velocity tensor, and performing correction calculations for the instantaneous tangential velocity. These steps reduce the method's real-time measurement capability, making it more suitable for data post-processing. Additionally, the radius vector estimation and instantaneous tangential velocity correction methods proposed in this paper can also be directly applied in situations where rotational motion information is obtained through additional equipment.

Although the method proposed in this paper significantly improves the accuracy of vessel velocity measurements, the improvement in displacement accuracy is limited. This is mainly because during free-swaying motion, much of the impact of the attitude dynamics is canceled out when integrating the vessel velocity. In cases of forced swaying or when influenced by waves, the symmetry of velocity fluctuations may be disrupted, potentially leading to larger displacement errors.

6. Conclusions

To correct for errors introduced by dynamic factors in attitude changes on a swaying platform without adding extra hardware, we propose an ADCP attitude dynamic error correction method based on angular velocity tensor and radius vector estimation. Compared with the conventional method, which only corrects static factors in attitude changes, the proposed method achieves greater velocity measurement accuracy and diminished fluctuations in swaying platform scenarios. Unlike other methods that necessitate extra devices, including INSs, differential GPSs, or AHRSs, to correct attitude dynamic errors, the proposed method minimizes the cost and complexity of flow measurements while enhancing flexibility and convenience. It also accounts for changes in tangential velocity and radial orientation during signal TX and RX. Experimental results indicate that, under both stationary and moving free-swaying conditions, the proposed method reduces the MRE by 73.81% and 20.94%, respectively, and decreases the RSD by 33.39% and 17.38%, respectively, compared with the ASC method. The proposed approach effectively corrects attitude dynamic errors in vessel velocity measurements.

Author Contributions: Z.S. designed the optimization methods, conducted the experiments, and wrote the draft of the manuscript. S.Y. and N.G. verified the optimization methods and reviewed and edited the manuscript. K.Z. verified the optimization methods. All authors have read and agreed to the published version of the manuscript.

Funding: This research was funded by the Fundamental Research Funds for the Central Universities through grant numbers 2242024K30004 and 2242023K5003.

Institutional Review Board Statement: Not applicable.

Informed Consent Statement: Not applicable.

Data Availability Statement: Data are contained within the article.

Acknowledgments: We would like to thank Yongshou Yang and Zheng Shen for their help during the experiments.

Conflicts of Interest: Author Ke Zhang was employed by the company Guobo Electronics Co., Ltd. The remaining authors declare that the research was conducted in the absence of any commercial or financial relationships that could be construed as a potential conflict of interest.

References

1. Dong, F.; Gao, H.; Liu, W.; Tan, C. Horizontal Oil-Water Two-Phase Dispersed Flow Velocity Profile Study by Ultrasonic Doppler Method. *Exp. Therm. Fluid Sci.* **2019**, *102*, 357–367. [\[CrossRef\]](#)
2. Prado, E.; Abad-Uribarren, A.; Ramo, R.; Sierra, S.; González-Pola, C.; Cristobo, J.; Ríos, P.; Graña, R.; Aierbe, E.; Rodríguez, J.M.; et al. Describing Polyps Behavior of a Deep-Sea Gorgonian, *Placogorgia* Sp., Using a Deep-Learning Approach. *Remote Sens.* **2023**, *15*, 2777. [\[CrossRef\]](#)
3. Rodríguez, E.; Wineteer, A.; Perkovic-Martin, D.; Gál, T.; Anderson, S.; Zuckerman, S.; Stear, J.; Yang, X. Ka-Band Doppler Scatterometry over a Loop Current Eddy. *Remote Sens.* **2020**, *12*, 2388. [\[CrossRef\]](#)
4. Gallagher, D.G.; Manley, R.J.; Hughes, W.W.; Pilcher, A.M. Development of an Enhanced Underwater Navigation Capability for Military Combat Divers. In Proceedings of the OCEANS 2016 MTS/IEEE Monterey, Monterey, CA, USA, 19–23 September 2016; pp. 1–4.
5. Titchenko, Y.; Jie, G.; Karaev, V.; Ponur, K.; Ryabkova, M.; Baranov, V.; Ocherednik, V.; He, Y. Preliminary Performance Assessment of the Wave Parameter Retrieval Algorithm from the Average Reflected Pulse. *Remote Sens.* **2024**, *16*, 418. [\[CrossRef\]](#)
6. Zhao, Y.-P.; Hangfei, L.; Bi, C.; Cui, Y.; Guan, C. Numerical Study on the Flow Field inside and around a Semi-Submersible Aquaculture Platform. *Appl. Ocean Res.* **2021**, *115*, 102824. [\[CrossRef\]](#)
7. Gao, Y.; Xie, X.; Li, G.; Hu, Z.; Xu, P.; Zhang, B.; Huang, H. Improving Accuracy of Horizontal Flow Field Using Acoustic Tomography with Real-Time Station Position Correction. *IEEE Trans. Instrum. Meas.* **2023**, *72*, 7501310. [\[CrossRef\]](#)
8. Zhu, L.; Lu, T.; Yang, F.; Wei, C.; Wei, J. Performance Assessment of a High-Frequency Radar Network for Detecting Surface Currents in the Pearl River Estuary. *Remote Sens.* **2024**, *16*, 198. [\[CrossRef\]](#)
9. Wang, Q.; Yang, H.; Wu, L.; Zhang, L.; Xia, Y.; Fu, X.; Tan, C. Complementary Coding-Based Waveform Design for Broadband Acoustic Doppler Current Profilers. *IEEE Trans. Veh. Technol.* **2024**, *73*, 9398–9410. [\[CrossRef\]](#)
10. Meurer, C.; Fuentes-Pérez, J.F.; Schwarzwälder, K.; Ludvigsen, M.; Sørensen, A.J.; Kruusmaa, M. 2D Estimation of Velocity Relative to Water and Tidal Currents Based on Differential Pressure for Autonomous Underwater Vehicles. *IEEE Robot. Autom. Lett.* **2020**, *5*, 3444–3451. [\[CrossRef\]](#)
11. Sun, Z.; Yao, S. Error Analysis and Correction of ADCP Attitude Dynamics under Platform Swing Conditions. *J. Mar. Sci. Eng.* **2024**, *12*, 1820. [\[CrossRef\]](#)
12. Velasco, D.W.; Nylund, S. Performance Improvement for ADCPs on Surface Buoys. In Proceedings of the 2019 IEEE/OES Twelfth Current, Waves and Turbulence Measurement (CWTM), San Diego, CA, USA, 10–13 March 2019; pp. 1–6.
13. Cusi, S.; Rodríguez, P.; Pujol, N.; Pairaud, I.; Nogueras, M.; Antonijuan, J.; Masmitja, I.; del Rio, J. Evaluation of AUV-Borne ADCP Measurements in Different Navigation Modes. In Proceedings of the OCEANS 2017, Aberdeen, Scotland, 19–22 June 2017; pp. 1–8.
14. Joseph, A. *Vertical Profiling of Currents Using Acoustic Doppler Current Profilers*; Elsevier: Amsterdam, The Netherlands, 2014; pp. 339–379, ISBN 978-0-12-415990-7.
15. Anderson, S.P.; Matthews, P. A Towed 75 kHz ADCP for Operational Deepwater Current Surveys. In Proceedings of the IEEE/OES Eighth Working Conference on Current Measurement Technology, Southampton, UK, 28–29 June 2005; pp. 46–49.
16. Stanway, M.J. Water Profile Navigation with an Acoustic Doppler Current Profiler. In Proceedings of the OCEANS'10 IEEE SYDNEY, Sydney, Australia, 24–27 May 2010; pp. 1–5.
17. Mueller, D.S. Assessment of Acoustic Doppler Current Profiler Heading Errors on Water Velocity and Discharge Measurements. *Flow Meas. Instrum.* **2018**, *64*, 224–233. [\[CrossRef\]](#)
18. Simpson, M.R. *Discharge Measurements Using a Broad-Band Acoustic Doppler Current Profiler*; United States Geological Survey: Sacramento, CA, USA, 2001.
19. Sarangapani, S. Multi-Frequency Phased Array Transducer for ADCP Applications. In Proceedings of the OCEANS 2022–Chennai, Chennai, India, 21–24 February 2022; pp. 1–10.
20. Herbers, T.H.C.; Lentz, S.J. Observing Directional Properties of Ocean Swell with an Acoustic Doppler Current Profiler (ADCP). *J. Atmos. Ocean. Technol.* **2010**, *27*, 210–225. [\[CrossRef\]](#)

21. Rennie, C.D. Non-Invasive Measurement of Fluvial Bedload Transport Velocity. Ph.D. Thesis, University of British Columbia, Vancouver, Canada, 2002.
22. Raye, R.E. *Characterization Study of the Florida Current at 26.11 North Latitude, 79.50 West Longitude for Ocean Current Power Generation*; Florida Atlantic University: Boca Raton, FL, USA, 2002.
23. Cao, Z. Research on the Technology of Acoustic Doppler Velocity Measurement for Underwater Vehicles. Ph.D. Thesis, Harbin Engineering University, Harbin, China, 2017.
24. Zhang, H.; Chen, Z.; Zhao, J.; Huang, J.; Wang, Z. ADCP Integration Measurement Based on External Sensor. *Geomat. Inf. Sci. Wuhan Univ.* **2016**, *41*, 1131–1136.
25. Yang, Y. Theory and Implementation of Acoustic Doppler Flow Measurement with Environmental Adaptability. Ph.D. Thesis, Southeast University, Jiangsu, China, 2023.
26. Fossen, T. *Handbook of Marine Craft Hydrodynamics and Motion Control*; John Wiley & Sons, Ltd.: Hoboken, NJ, USA, 2011; ISBN 978-1-119-99413-8.
27. Faltinsen, O.M. *Sea Loads on Ships and Offshore Structures*; Cambridge University Press: Cambridge, UK; New York, NY, USA, 1990; ISBN 978-0-521-37285-5.

Disclaimer/Publisher's Note: The statements, opinions and data contained in all publications are solely those of the individual author(s) and contributor(s) and not of MDPI and/or the editor(s). MDPI and/or the editor(s) disclaim responsibility for any injury to people or property resulting from any ideas, methods, instructions or products referred to in the content.